BIOCHEMISTRY

Immunomodulatory actions of a kynurenine-derived endogenous electrophile

Mara Carreño[1]†, Maria F. Pires[1]†, Steven R. Woodcock[1], Tomasz Brzoska[2,3], Samit Ghosh[2,3], Sonia R. Salvatore[1], Fei Chang[1], Nicholas K. H. Khoo[1,4], Matthew Dunn[1], Nora Connors[1], Shuai Yuan[2], Adam C. Straub[1,2,5], Stacy G. Wendell[1,4], Gregory J. Kato[6], Bruce A. Freeman[1], Solomon F. Ofori-Acquah[2,3,7], Prithu Sundd[2,3,8], Francisco J. Schopfer[1,2,4], Dario A. Vitturi[1,2,9]*

The up-regulation of kynurenine metabolism induces immunomodulatory responses via incompletely understood mechanisms. We report that increases in cellular and systemic kynurenine levels yield the electrophilic derivative kynurenine-carboxyketoalkene (Kyn-CKA), as evidenced by the accumulation of thiol conjugates and saturated metabolites. Kyn-CKA induces NFE2 like bZIP transcription factor 2– and aryl hydrocarbon receptor–regulated genes and inhibits nuclear factor κB– and NLR family pyrin domain containing 3-dependent proinflammatory signaling. Sickle cell disease (SCD) is a hereditary hemolytic condition characterized by basal inflammation and recurrent vaso-occlusive crises. Both transgenic SCD mice and patients with SCD exhibit increased kynurenine and Kyn-CKA metabolite levels. Plasma hemin and kynurenine concentrations are positively correlated, indicating that Kyn-CKA synthesis in SCD is up-regulated during pathogenic vascular stress. Administration of Kyn-CKA abrogated pulmonary microvasculature occlusion in SCD mice, an important factor in lung injury development. These findings demonstrate that the up-regulation of kynurenine synthesis and its metabolism to Kyn-CKA is an adaptive response that attenuates inflammation and protects tissues.

INTRODUCTION

Acute and chronic inflammation induces the rate-limiting enzymes indoleamine 2,3-dioxygenase-1 (IDO1) and tryptophan 2,3-dioxygenase (TDO2) that in turn increase kynurenine and kynurenine/tryptophan ratios (*1*). Increased kynurenine synthesis via TDO2 in hepatocytes is protective against primary endotoxemia, while IDO1 induction in myeloid leukocytes attenuates inflammatory responses to endotoxin, promotes the generation of tolerogenic dendritic cells, and facilitates regulatory T cell polarization (*2*–*5*). Consistent with these immunomodulatory effects, dysregulated kynurenine metabolism occurs in inflammatory conditions such as cardiovascular disease, cancer, renal injury, and transplantation and is often a strong predictor of outcome (*6*–*9*). However, despite its pathophysiological relevance, the mechanisms responsible for the immunoregulatory effects of kynurenine and its metabolites are poorly defined (*10*).

Biological electrophiles contain carbon-carbon double bonds conjugated to electron-withdrawing moieties that generate electron-deficient carbons that are susceptible to nucleophilic attack by thiols or, less predominantly, amines (*11*). Covalent modification of critical cysteine thiols in transcription factors, signaling proteins, and metabolic enzymes has profound effects on cellular function (*11*). In particular, reactive electrophiles elicit cytoprotective and immunomodulatory effects both preclinically and clinically by up-regulating NFE2 like bZIP transcription factor 2 (Nrf2)–dependent antioxidant enzyme translation and inhibiting nuclear factor κB (NF-κB)–dependent gene expression and inflammatory cell metabolic reprogramming (*11*, *12*). Kynurenine deaminates in solution to generate an electrophilic α,β-unsaturated carbonyl-containing product, kynurenine-carboxyketoalkene (Kyn-CKA), which participates in the generation of ultraviolet (UV) filters in the eye lens (*13*–*17*). Critically, the potential for Kyn-CKA to contribute to the immunomodulatory actions of kynurenine metabolites has not been explored.

Here, we show that kynurenine synthesis in hepatocytes and macrophages generates Kyn-CKA. Kyn-CKA–specific metabolites detected in healthy humans and mice affirm that Kyn-CKA formation occurs biologically, with Kyn-CKA generation up-regulated by increases in systemic kynurenine concentrations. Kyn-CKA activates Nrf2- and aryl hydrocarbon receptor (AhR)–dependent gene expression and inhibits NF-κB– and NLR family pyrin domain containing 3 (NLRP3)-dependent proinflammatory responses in both parenchymal and immune cells. These responses are recapitulated across several tissues in vivo. In addition to up-regulating Nrf2- and AhR-dependent signaling under basal nonactivated conditions, Kyn-CKA attenuates lipopolysaccharide (LPS)–induced proinflammatory gene expression and cytokine synthesis. Last, Kyn-CKA increases interleukin-10 (IL-10) levels and attenuates the expression of renal injury markers in LPS-treated mice, suggesting potent anti-inflammatory and cytoprotective actions in vivo.

The anti-inflammatory effects of Kyn-CKA suggested the possibility that its formation might constitute a missing link in kynurenine signaling and an adaptive immunomodulatory response having the potential to modulate disease progression. To test this hypothesis, we focused on the hemolytic inflammatory conditions intrinsic to sickle cell disease (SCD), wherein the activation of endothelial, platelet, and leukocyte Toll-like receptor 4 (TLR4) by hemoglobin-derived products promotes the formation of multicellular aggregates that, in combination with increased sickle erythrocyte

[1]Department of Pharmacology and Chemical Biology, University of Pittsburgh, Pittsburgh, PA, USA. [2]Pittsburgh Heart, Lung and Blood Vascular Medicine Institute, University of Pittsburgh, Pittsburgh, PA, USA. [3]Division of Hematology/Oncology, Department of Medicine, University of Pittsburgh, Pittsburgh, PA, USA. [4]Pittsburgh Liver Research Center, University of Pittsburgh, Pittsburgh, PA, USA. [5]Center for Microvascular Research, University of Pittsburgh, Pittsburgh, PA, USA. [6]CSL Behring, King of Prussia, PA, USA. [7]School of Biomedical and Allied Health Sciences, University of Ghana, Accra, Ghana. [8]Department of Bioengineering, University of Pittsburgh, Pittsburgh, PA, USA. [9]Center for Critical Care Nephrology, University of Pittsburgh, Pittsburgh, PA, USA.
*Corresponding author. Email: dav28@pitt.edu
†These authors contributed equally to this work.

rigidity and adhesiveness, cause vaso-occlusion and ischemic injury. This phenomenon not only causes severe pain crises but also leads to the development of life-threatening acute and chronic complications (*18*, *19*). Analysis of plasma samples obtained from a transgenic humanized SCD mouse model and from patients with SCD showed elevated kynurenine levels that correlated positively with proinflammatory plasma hemin concentrations. This increased kynurenine synthesis was further correlated with greater Kyn-CKA metabolite concentrations in the plasma and urine of SCD mice and patients with SCD. Quantitative fluorescence intravital microscopy was used to monitor vaso-occlusive occurrence in the lung microvasculature of SCD mice and to test the role of Kyn-CKA as a modulator of tissue dysfunction (*20*, *21*). Consistent with a role as an endogenous anti-inflammatory mediator in SCD, Kyn-CKA significantly decreased the average size of multicellular aggregates and inhibited vaso-occlusion of the pulmonary microvasculature.

Collectively, our results reveal that Kyn-CKA is present under basal conditions and that its formation is adaptively elevated within the context of inflammatory kynurenine synthesis up-regulation. Kyn-CKA is an endogenous electrophilic signaling mediator capable of attenuating proinflammatory signaling cascades, modulating complex pathological responses, and potentially affecting the course of human disease.

RESULTS

Kynurenine yields Kyn-CKA and promotes Nrf2- and AhR-dependent gene expression

Kynurenine is a main product of tryptophan metabolism and, upon deamination, is activated into Kyn-CKA, an α,β-unsaturated carbonyl-containing derivative with electrophilic reactivity (Fig. 1A). Treatment of the mouse hepatocyte cell line AML-12 with Kyn-CKA dose-dependently up-regulated electrophile-sensitive Nrf2-dependent gene expression both at the transcript and protein levels (Fig. 1, B and C), a response that is inhibited in embryonic fibroblasts derived from *Nrf2*$^{-/-}$ mice [mouse embryonic fibroblast (MEF); fig. S1, A to C]. Furthermore, Kyn-CKA induced the expression of the AhR-regulated products *CYP1A1* and *CYP1B1* (Fig. 1D), while marginal AhR engagement was observed with L-kynurenine (L-Kyn) at the same doses and incubation times (fig. S1D). Kyn-CKA contains a nucleophilic aromatic amine that can react intramolecularly with the α,β-unsaturated carbonyl moiety, giving rise to a cyclized derivative known as Kyn-Yellow (*15*). While the nonelectrophilic Kyn-Yellow is unable to promote Nrf2-dependent gene expression, it remained equally potent as an AhR ligand (fig. S1, E to H). This finding is consistent with recent reports indicating that AhR activation by kynurenine is at least in part dependent on the generation of planar

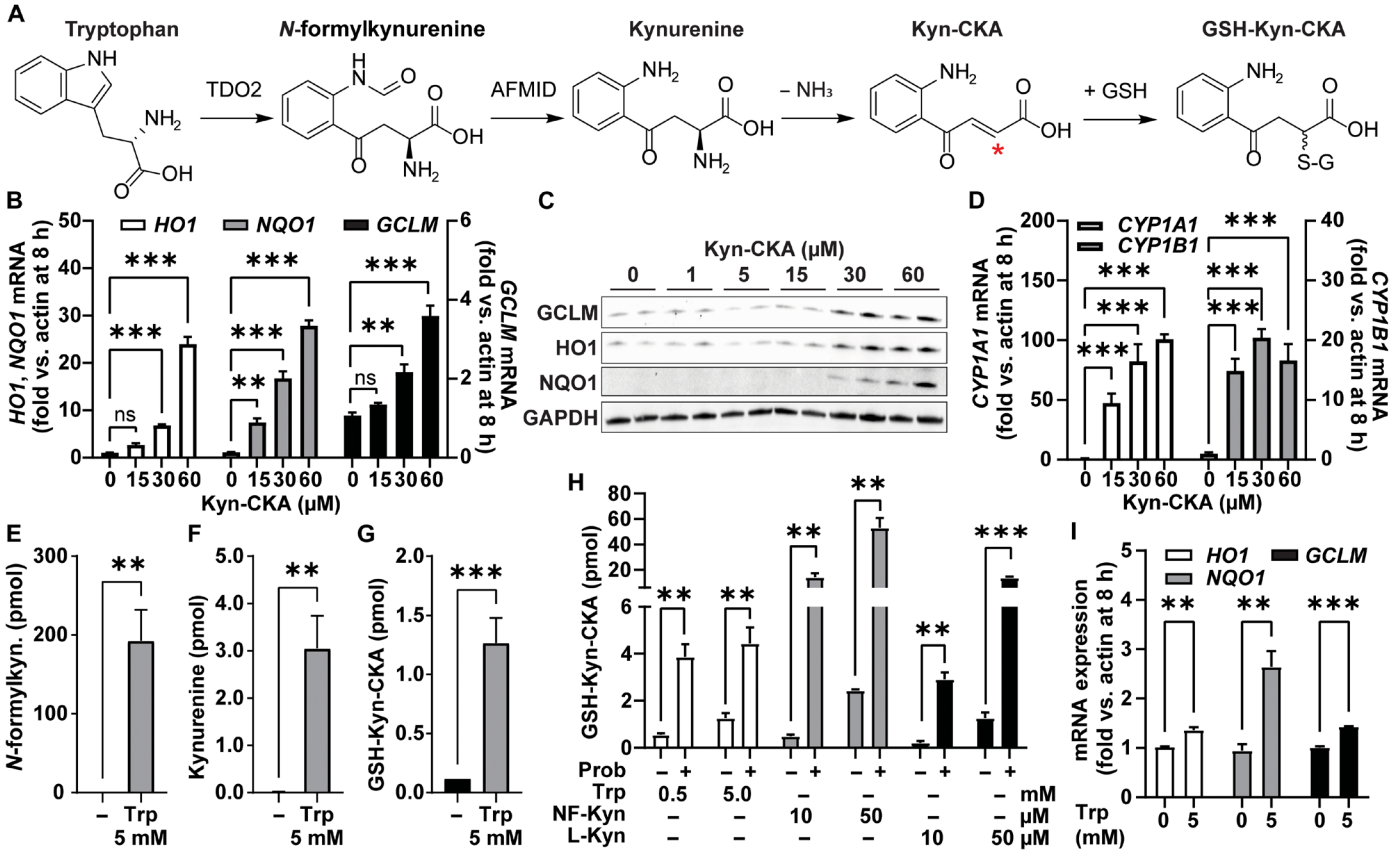

Fig. 1. Bioactive Kyn-CKA is formed following kynurenine synthesis in AML-12 cells. (**A**) Proposed route for Kyn-CKA formation following from tryptophan (Trp) metabolism. The asterisk denotes the electrophilic carbon. TDO2, tryptophan 2,3-dioxygenase; AFMID, arylformamidase. (**B**) Nrf2-dependent gene induction by Kyn-CKA ($n = 3$). (**C**) Nrf2-regulated protein expression 24 hours after Kyn-CKA. (**D**) Activation of AhR-dependent genes by 8-hour Kyn-CKA treatment. (**E** to **G**) Kynurenine pathway metabolites 8 hours after tryptophan in HBSS (5 mM; $n = 3$). (**H**) GSH-Kyn-CKA formation 8 hours after *N*-formylkynurenine (NF-Kyn) or L-Kyn in HBSS in the presence or absence of 1 mM probenecid (Prob) ($n = 3$ per dose). (**I**) Nrf2-dependent gene expression 8 hours after tryptophan in HBSS ($n = 3$). $^{**}P < 0.01$ and $^{***}P < 0.0001$ by one-way analysis of variance (ANOVA) and Tukey's test (B and D) or by *t* test (E to I). ns, not significant.

condensation derivatives (*22*). Together, our results demonstrate that Kyn-CKA is a chemically and biologically active product.

To define the contribution of intracellular enzymatic reactions to the endogenous formation of Kyn-CKA, AML-12 cells were treated with tryptophan (5 mM) for 8 hours in Hanks' balanced salt solution (HBSS), and the levels of the intermediate metabolites *N*-formylkynurenine and kynurenine were assessed. Tryptophan caused a significant increase in *N*-formylkynurenine and kynurenine synthesis that led to the formation of glutathione (GSH) conjugates of Kyn-CKA (GSH-Kyn-CKA) (Fig. 1, E to G). Similarly, treatment with *N*-formylkynurenine (10 and 50 μM) or L-Kyn (10 and 50 μM) resulted in dose-dependent GSH-Kyn-CKA formation (Fig. 1H). The formation of GSH conjugates is the first step in the mercapturic acid pathway, a conserved mechanism for cellular electrophile inactivation that is followed by export through multidrug resistance proteins (MRPs) (*23*). In this regard, treatment with the pan-MRP inhibitor probenecid induced significant increases in intracellular GSH-Kyn-CKA levels (Fig. 1H). Consistent with its high electrophilic reactivity, intracellular non–thiol-adducted Kyn-CKA was not detected.

The treatment of AML-12 cells with tryptophan results in the formation of GSH-Kyn-CKA adducts and significant induction of Nrf2-dependent gene expression (Fig. 1I). This underscores the concept that intracellularly formed Kyn-CKA can evade both high cellular GSH concentrations and excretion by the mercapturic acid pathways to induce kelch like ECH associated protein 1 (Keap1) thiol alkylation and promote Nrf2-regulated signaling. Estimating an approximate AML-12 monolayer volume of 6 μl based on a cellular volume of ~3×10^{-12} liters per cell and 2×10^6 cells per well, the yields of intracellular GSH-Kyn-CKA adducts obtained following exogenous precursor supplementation ranged from ~30 to 400 nM in the absence of probenecid and to up to ~8.5 μM when MRPs were inhibited. These results indicate that intracellularly generated Kyn-CKA induces cell signaling responses at lower concentrations than when added exogenously. In line with these findings, the cell-permeable analog *N*-octanoyl–Kyn-CKA induced Nrf2-dependent gene expression at lower concentrations than its cell-impermeable precursor (fig. S1, I to L), thus demonstrating that membrane transport is a major determinant of the potency of extracellular Kyn-CKA.

In vivo generation of Kyn-CKA

In vivo, intracellular electrophile-GSH conjugates are exported and metabolized to yield cysteine and mercapturic acid conjugates that are excreted in urine (*23*). To evaluate Kyn-CKA-specific metabolites in vivo, urine was collected from C57Bl/6J mice either in the absence or 8 hours following Kyn-CKA supplementation [20 and 50 mg/kg, intraperitoneally (ip)]. Consistent with its endogenous nature, liquid chromatography–tandem mass spectrometry (LC-MS/MS) analyses demonstrated the presence of urinary Cys-Kyn-CKA adducts in untreated mice, which was confirmed by coelution with a synthetic $^{13}C_3$-Cys-Kyn-CKA standard (Fig. 2A). Exogenous Kyn-CKA administration gave higher levels of urinary Cys-Kyn-CKA adducts and led to the excretion of *N*-acetyl-cysteine Kyn-CKA conjugates (NAC-Kyn-CKA; Fig. 2B and fig. S2). In addition, liver tissue analysis revealed endogenous GSH-Kyn-CKA adducts in untreated mice, with GSH-Kyn-CKA significantly increased by Kyn-CKA treatment (Fig. 2, C and D, and fig. S2). These results were recapitulated in C57Bl/6J treated with L-Kyn, suggesting that systemic increases in this amino acid metabolite can promote Kyn-CKA formation in vivo (Fig. 2, E and F). Untargeted analysis of plasma samples from Kyn-CKA–treated mice revealed unadducted Kyn-CKA together with several up-regulated LC-MS/MS features, including a reduced carboxyketoalkane derivative termed Red-Kyn-CKA (Fig. 2G and fig. S3). Red-Kyn-CKA formation from Kyn-CKA was validated using a rat liver S9 fraction and reduced nicotinamide adenine dinucleotide phosphate (NADPH) as a source of reducing equivalents (fig. S3) and confirmed by comparing the MS/MS fragmentation pattern with a synthetic standard (Fig. 2H). Unlike urinary and hepatic conjugates, neither free Kyn-CKA nor Red-Kyn-CKA was detected in untreated mouse plasma. Transcript expression analysis from Kyn-CKA–treated mice revealed induction of Nrf2-dependent signaling in the kidneys, heart, and liver (Fig. 2, I to K) as confirmed at the protein level in the liver and kidneys (Fig. 2, L and M). Although changes in *CYP1A1* expression did not reach statistical significance, Kyn-CKA induced the expression of *CYP1B1* in the liver (fig. S4). No transcriptional changes were observed in the lung and brain. Nrf2- and AhR-dependent gene expression was also up-regulated in the liver of L-Kyn–treated mice, consistent with Kyn-CKA formation in this tissue (Fig. 2N and fig. S4) and reinforced by both increased levels of hepatic GSH-Kyn-CKA and urinary Cys-Kyn-CKA conjugates (Fig. 2, E and F). Notably, the doses of L-Kyn selected here are comparable to those used in the literature to demonstrate an immunomodulatory and cytoprotective role for the kynurenine pathway in vivo (*2*, *24*, *25*).

Kyn-CKA inhibits NF-κB–dependent signaling and NLRP3 inflammasome engagement in macrophages

While TDO2 catalyzes kynurenine synthesis in the liver, this reaction is mediated by IDO1 in myeloid cells. Akin to the results obtained with AML-12 hepatocytes, tryptophan treatment of J774a.1 macrophages increased the formation of *N*-formylkynurenine and kynurenine, as well as GSH-Kyn-CKA (Fig. 3, A and C). In addition to inducing Nrf2-dependent gene expression (fig S5A), Kyn-CKA inhibited the LPS-induced expression of proinflammatory cytokines and enzymes that generate nitrogen oxides in both J774a.1 (Fig. 3, D to H) and bone marrow–derived macrophages (BMDMs; fig. S5, B to F). Time-dependent analysis of LPS-induced inhibitor of NF-κBα (IκBα) phosphorylation and degradation in J774a.1 cells revealed that while Kyn-CKA treatment had no substantial impact on the early response to TLR4 engagement, it still decreased nuclear p65 levels at 2 and 6 hours (Fig. 3, I and J, and fig. S5, G and H). Notably, binding affinity analysis demonstrated that Kyn-CKA inhibits purified p65 association with its consensus DNA sequence in a dose-dependent manner (Fig. 3K). No changes in AhR-dependent gene expression were detected in J774a.1 cells, and no effect was observed on LPS responses by either Kyn-Yellow or the prototypical AhR ligand 2,3,7,8-tetrachlorodibenzodioxin (TCDD), suggesting that the anti-inflammatory effects of Kyn-CKA are independent of this pathway (fig. S5, I to L). However, Kyn-CKA did induce *CYP1A1* expression in BMDM (fig. S5M). NF-κB activation is essential in priming the NLRP3 inflammasome via increased synthesis of NLRP3 subunits and pro–IL-1β. Activation of the primed inflammasome promotes proteolytic pro–caspase-1 activation, followed by mature IL-1β generation (*12*). Kyn-CKA treatment of LPS/adenosine 5′-triphosphate (ATP)–activated J774a.1 dose-dependently inhibited NLRP3 and pro–IL-1β expression and attenuated pro–caspase-1 levels to inhibit processing and secretion

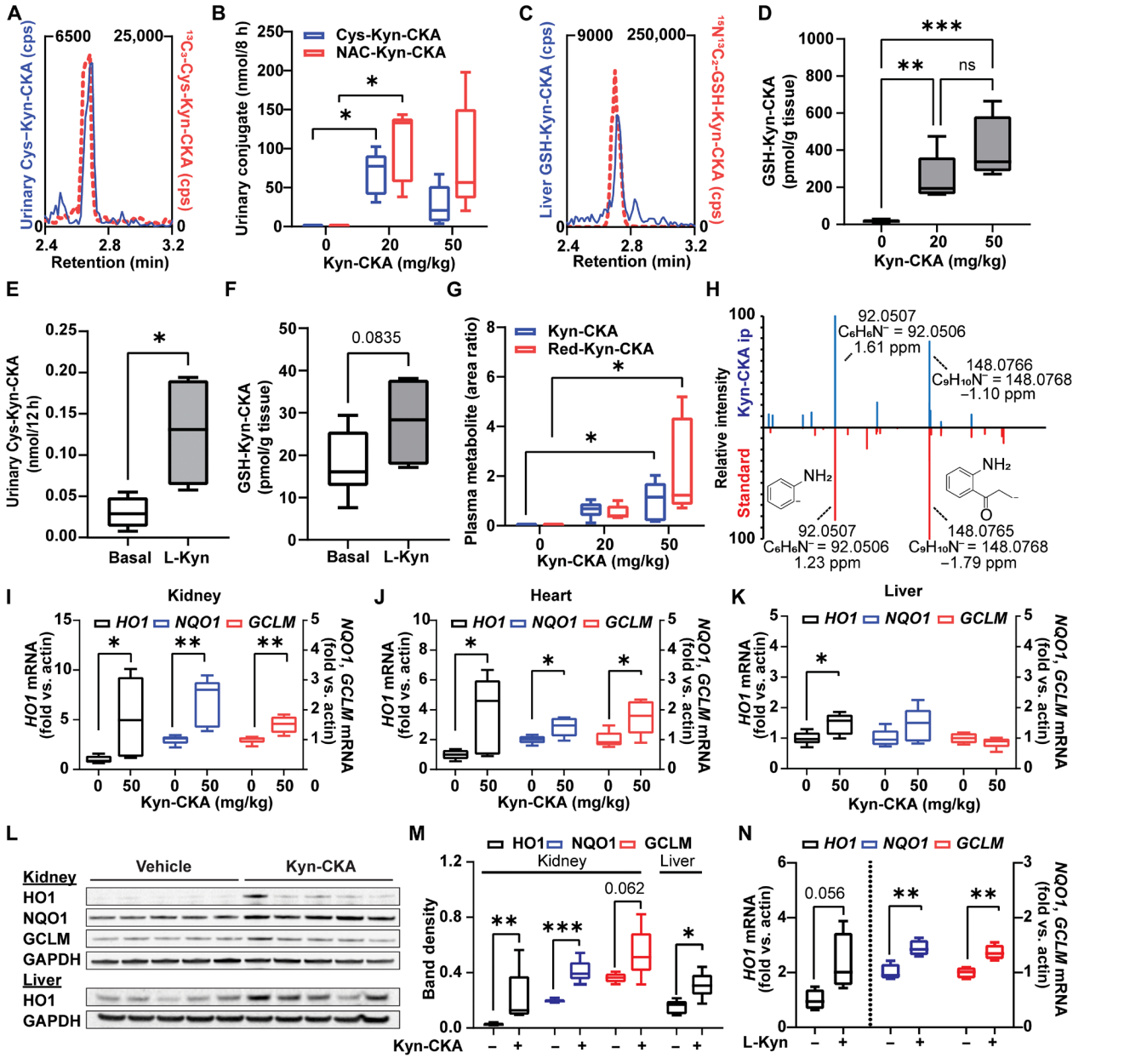

Fig. 2. Kyn-CKA is formed endogenously and induces Nrf2-dependent genes in vivo. (**A**) Representative LC-MS/MS trace showing coelution between endogenous urinary Cys-Kyn-CKA and an isotopically labeled synthetic standard. cps, counts per second. (**B**) Urinary Cys-Kyn-CKA and NAC-Kyn-CKA 8 hours after Kyn-CKA (intraperitoneally) in C57Bl6/J mice ($n = 5$ per dose). (**C**) LC-MS/MS trace of endogenous GSH-Kyn-CKA in the untreated mouse liver coeluting with an isotopically labeled synthetic standard. (**D**) Hepatic GSH-Kyn-CKA in mice 8 hours following Kyn-CKA (basal, $n = 9$; $n = 5$ per dose). (**E**) Urinary Cys-Kyn-CKA in mice receiving L-Kyn (50 mg/kg/day, ip, two doses, 24 hours apart $n = 4$). (**F**) Hepatic GSH-Kyn-CKA L-Kyn–treated mice (50 mg/kg/day, ip, two doses, 24 hours apart; basal, $n = 9$; L-Kyn, $n = 4$). (**G**) Plasma Kyn-CKA metabolites 8 hours after dosing. (**H**) Red-Kyn-CKA MS/MS spectra for Kyn-CKA–treated plasma (20 mg/kg, above) and synthetic Red-Kyn-CKA (below). (**I** to **K**) Nrf2-dependent gene expression in mice 8 hours after Kyn-CKA (50 mg/kg; $n = 5$ per dose). (**L** and **M**) Nrf2-dependent protein levels in mice 24 hours after Kyn-CKA (25 mg/kg, ip, two doses, 8 hours apart). (**N**) Nrf2-dependent gene expression in the mouse liver 12 hours after second L-Kyn dose (50 mg/kg, ip, two doses, 24 hours apart; $n = 4$). $^*P < 0.05$, $^{**}P < 0.01$, and $^{***}P < 0.0001$ by one-way ANOVA and Tukey's test (B, D, and G) or t test (E, F, and I to N). Kidney HO1 in (M) was analyzed by Mann-Whitney test.

of mature IL-1β (Fig. 3L), with similar results obtained using BMDM (fig. S5N). Last, Kyn-CKA also inhibited LPS-induced vascular cell adhesion molecule–1 (VCAM-1) expression in human pulmonary microvascular endothelial cells, supporting that Kyn-CKA can invoke systemic anti-inflammatory responses across different cell types and tissues (fig. S5O).

To determine whether the anti-inflammatory effects of Kyn-CKA in vitro translate to in vivo inflammatory scenarios, C57Bl6/J mice were treated with a single dose of Kyn-CKA (50 mg/kg, ip), followed by LPS challenge 30 min later (10 mg/kg, ip). The Kyn-CKA dose was chosen on the basis of literature precedent for the structurally similar but cell-permeable electrophile dimethylfumarate (*26*, *27*).

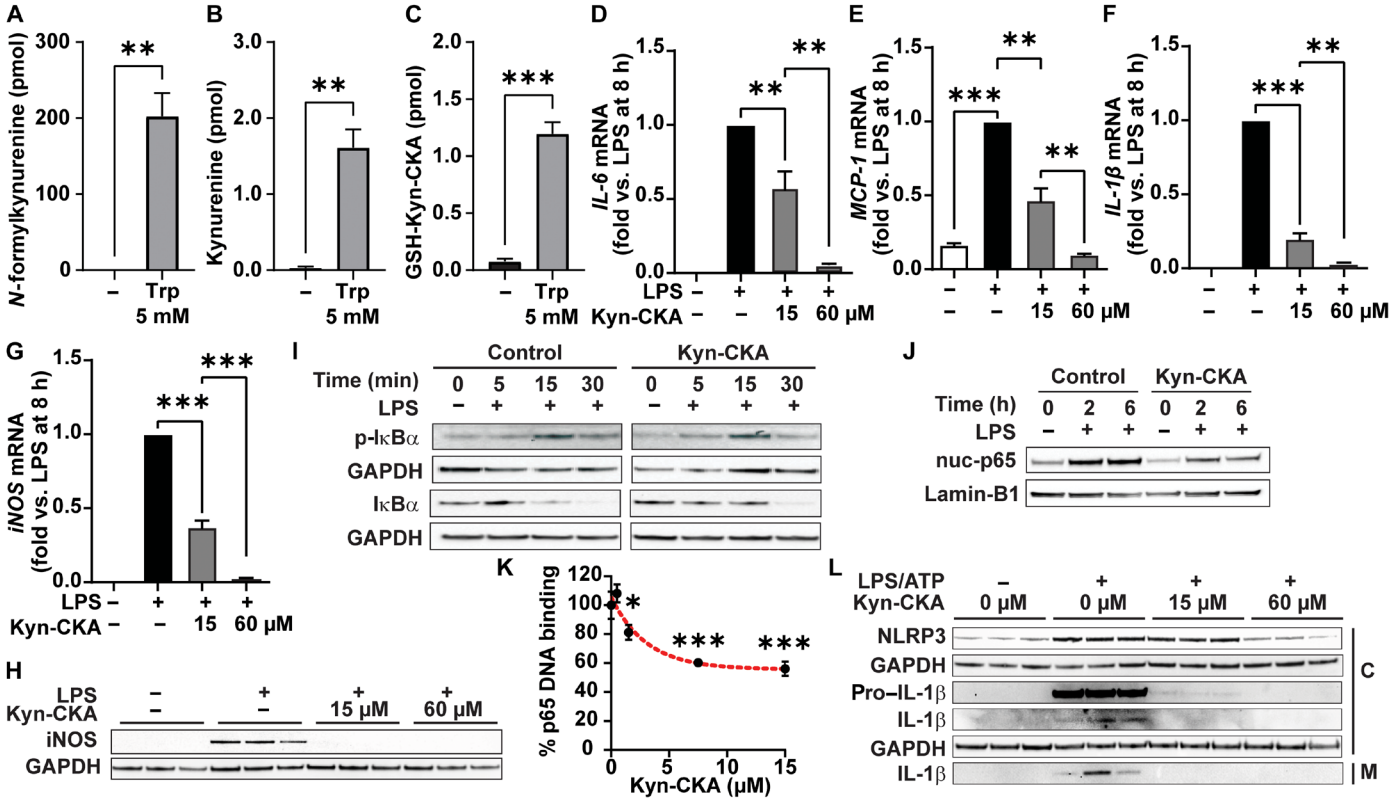

Fig. 3. Kyn-CKA is formed and attenuates NF-κB and NLRP3 signaling in macrophages. (**A** to **C**) Kynurenine metabolites in J774a.1 8 hours after tryptophan (5 mM; $n = 3$). (**D** to **G**) NF-κB–dependent gene expression 8 hours after LPS (1 μg/ml) and Kyn-CKA (15 or 60 μM; $n = 3$). (**H**) Inducible nitric oxide synthase (iNOS) levels 8 hours after LPS (1 μg/ml) and Kyn-CKA. (**I**) Total and phospho (p)–IκBα following LPS in the presence of Kyn-CKA (0 or 30 μM). (**J**) Nuclear p65 (nuc-p65) in LPS-treated J774a1 versus time and Kyn-CKA (0 or 30 μM); each lane are three combined independent wells. (**K**) p65 (1.5 μM) DNA binding versus Kyn-CKA ($n = 3$ per concentration). Nonlinear fit provided for illustration purposes. (**L**) Inhibition of NLRP3 inflammasome activation by LPS/ATP (1 μg/ml; ATP, 2 mM) by Kyn-CKA at 8 hours. C, cellular fraction; M, media. *$P < 0.05$, **$P < 0.01$, and ***$P < 0.0001$ by t test (A to C) or one-way ANOVA and Tukey's test (D to G and K).

Tissue NF-κB–dependent gene expression revealed anti-inflammatory responses to Kyn-CKA in the kidneys (Fig. 4, A to D), heart (Fig. 4, E to H), and lung (Fig. 4I). Kyn-CKA pretreatment also decreased the expression of the renal injury marker *KIM-1*, affirming attenuation of LPS-induced acute kidney injury (Fig. 4J). Consistent with the induction of systemic anti-inflammatory responses, Kyn-CKA significantly inhibited plasma levels of several proinflammatory cytokines (Fig. 4, K to O) while increasing the anti-inflammatory mediator IL-10 (Fig. 4P).

Kyn-CKA levels are elevated in SCD, and Kyn-CKA administration attenuates inflammatory vaso-occlusion

To define the potential contributions of Kyn-CKA formation under clinically relevant pathological conditions, the concentrations of Kyn-CKA metabolites were determined in a humanized mouse model of SCD. Compared to nonsickle HbAA controls, homozygous HbSS mice exhibited higher hepatic TDO2 expression and elevated plasma kynurenine levels (Fig. 5, A to C). A strong positive correlation was observed between kynurenine and hemin concentrations in HbSS mouse plasma, indicating an association between pathogenic hemin accumulation and kynurenine synthesis (Fig. 5D). In this regard, while hemin failed to induce *TDO2* in AML-12 hepatocytes, it up-regulated *IDO1* expression in J774a.1 macrophages (Fig. 5E). Consistent with increased Kyn-CKA formation secondary to kynurenine synthesis, urinary Cys-Kyn-CKA levels were significantly greater in HbSS versus HbAA mice (Fig. 5F). This was recapitulated clinically in a cohort of patients with SCD that, in addition to greater plasma kynurenine concentrations, also exhibited increased levels of both urinary Cys-Kyn-CKA and plasma Red-Kyn-CKA (Fig. 5, G to I). No differences in circulating tryptophan levels were observed between SCD and non-SCD subjects in either mouse or human cohorts, and kynurenine to tryptophan ratios were consistent with kynurenine pathway up-regulation in SCD (fig. S6).

To test whether the anti-inflammatory actions of Kyn-CKA can modulate SCD-specific pathology, inflammatory vaso-occlusion was monitored in real time by intravital microscopy of the pulmonary microvasculature (*20*, *21*). Intravenous injection of a nanogram dose of LPS (0.1 μg/kg) in HbSS mice promoted formation of multicellular aggregates composed of platelets and neutrophils that obstructed pulmonary arterioles and led to the interruption of blood flow in the lung. Pretreatment with Kyn-CKA [10 mg/kg, intravenously (iv)] significantly inhibited both pulmonary vaso-occlusion and the size of individual multicellular aggregates (Fig. 5, J to L, and Supplementary Media). These results reinforce that Kyn-CKA formation secondary to kynurenine synthesis up-regulation in SCD is an adaptive anti-inflammatory response that inhibits inflammatory events leading to vaso-occlusion and protects organs against the cumulative effects of recurrent metabolic and physical stresses.

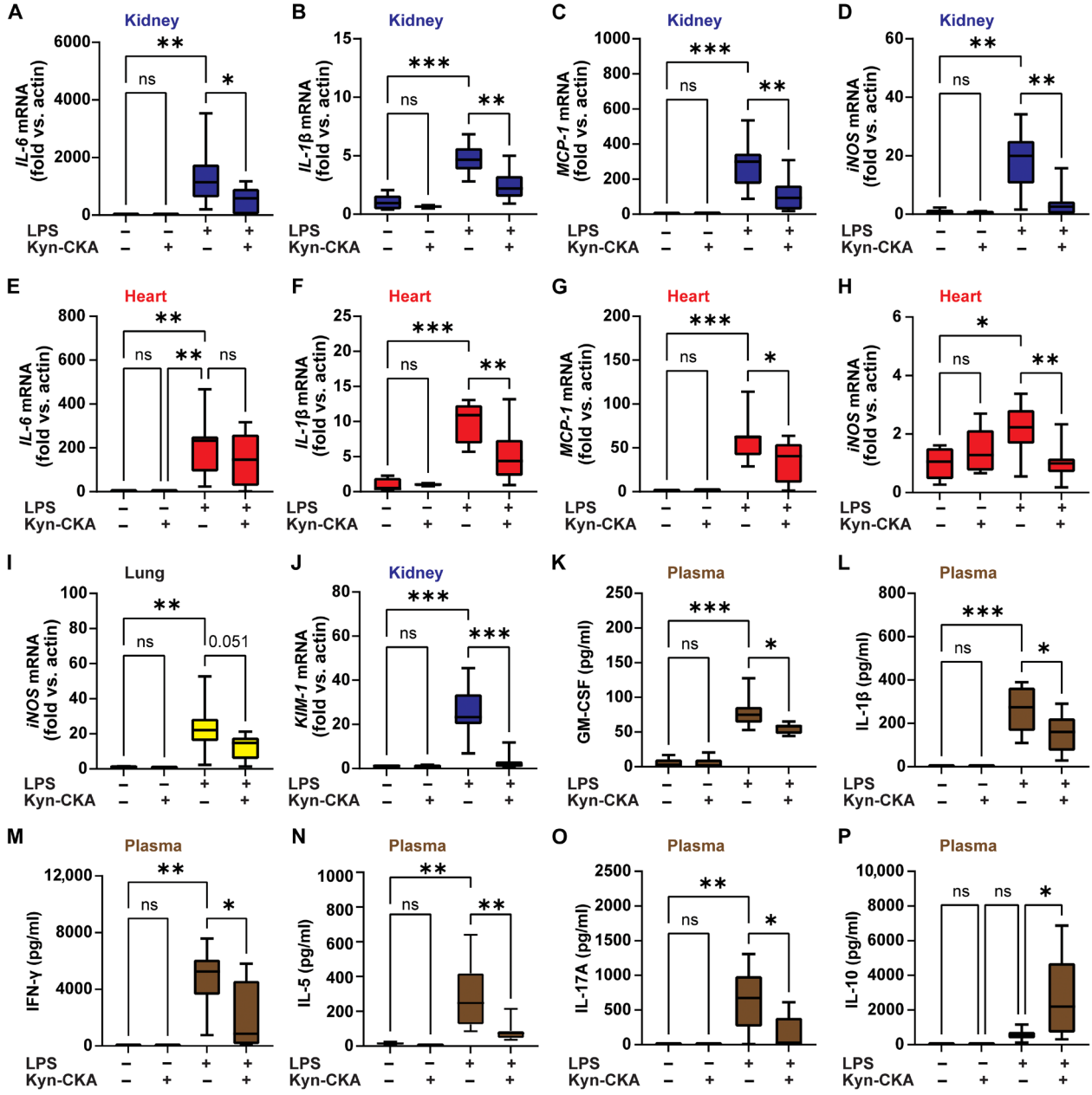

Fig. 4. Kyn-CKA promotes anti-inflammatory actions in vivo. (**A** to **I**) Kyn-CKA (50 mg/kg, ip, 30 min before challenge) inhibits NF-κB target gene expression 8 hours after LPS (10 mg/kg, ip). (**J**) Kyn-CKA inhibits *KIM-1* 8 hours following LPS. (**K** to **P**) Plasma cytokine levels modulated by Kyn-CKA 8 hours after LPS. Non-LPS–treated ($n = 5$) and LPS-treated ($n = 8$ to 9). $^{*}P < 0.05$, $^{**}P < 0.01$, and $^{***}P < 0.001$ by one-way ANOVA and Tukey's test.

DISCUSSION

The up-regulation of the rate-limiting enzymes in kynurenine metabolism is linked with diverse anti-inflammatory and immunomodulatory effects, but the precise mechanisms behind these immunosuppressive actions are incompletely understood (*10*). Proposed effects include TDO2- or IDO1-mediated decreases in tryptophan, alterations in nicotinamide adenine dinucleotide availability, activity-independent signaling actions of IDO1, and the generation of bioactive kynurenine metabolites (*2*, *10*, *28*). In particular, the activation of the AhR and the G protein–coupled receptor 35 by kynurenine and kynurenic acid have been proposed, but whether their physiological concentrations are sufficient to engage these pathways in vivo is controversial (*22*, *29*). Here, we demonstrate that kynurenine yields a bioactive electrophile, Kyn-CKA, in vitro and in vivo. Moreover, the anti-inflammatory signaling actions of Kyn-CKA suggest that this previously unidentified metabolite could account for a substantial fraction of the immunomodulatory effects ascribed to the kynurenine pathway.

A facile reaction with abundant nucleophilic thiols and amines, combined with substantial metabolic transformation, makes the in vivo detection of endogenous Kyn-CKA in its "free" nonadducted form highly challenging. As a result, strategies for highly reactive

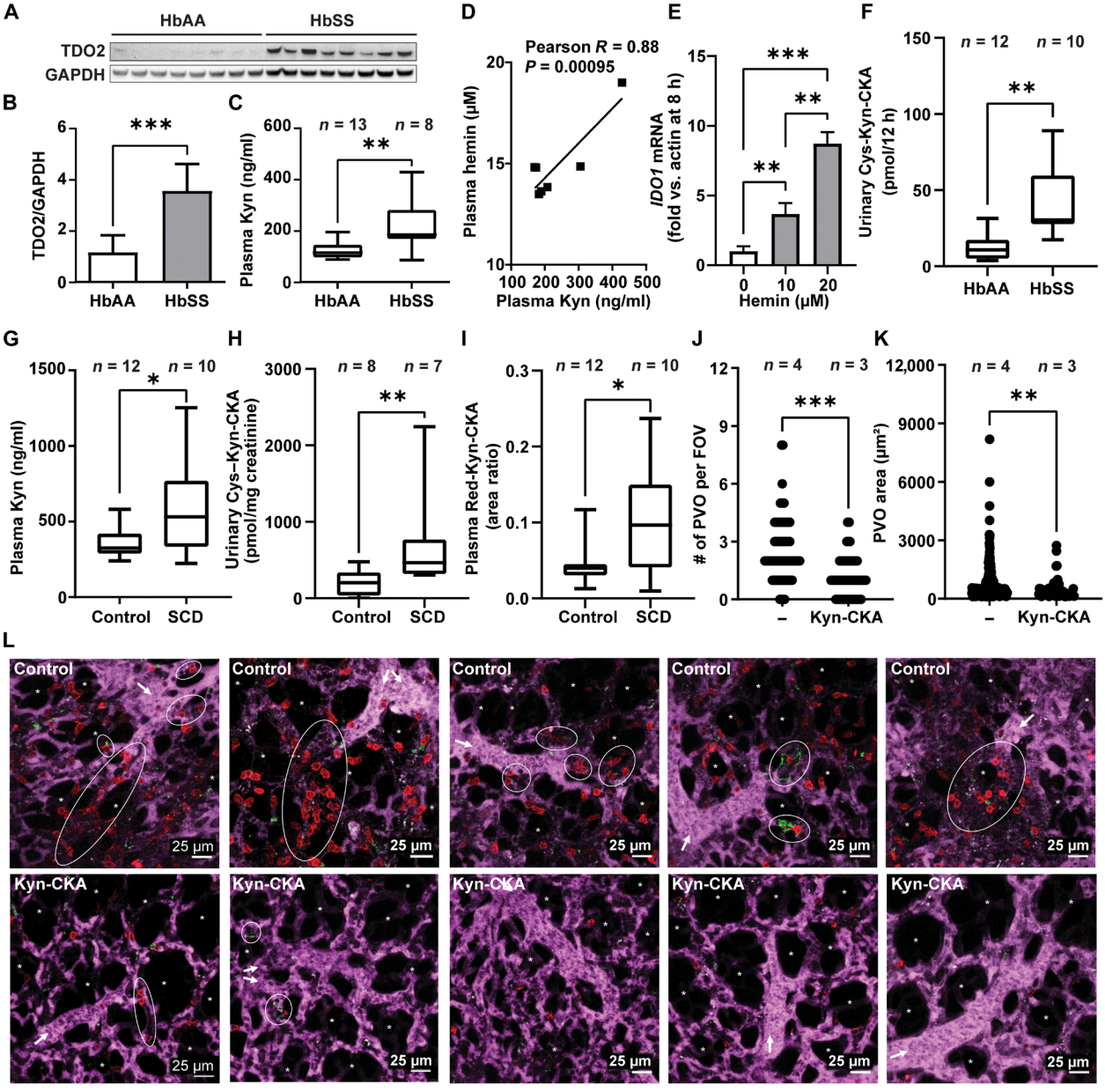

Fig. 5. Kyn-CKA synthesis is elevated in SCD and attenuates pulmonary microvascular occlusion. (**A** and **B**) TDO2 immunoblot and quantification ($n = 8$ per genotype). (**C**) Plasma kynurenine in HbAA versus HbSS mice. (**D**) Correlation between HbSS plasma kynurenine and hemin ($n = 7$). (**E**) *IDO1* induction by hemin in J774a.1 ($n = 3$ per condition). (**F**). Cys-Kyn-CKA in 12 hours HbAA and HbSS urine. (**G** to **I**) Plasma kynurenine, urinary Cys-Kyn-CKA, and plasma Red-Kyn-CKA in healthy and SCD volunteers. (**J** and **K**) Number of pulmonary vaso-occlusions (PVO) per field of view (FOV) and pulmonary vaso-occlusion area in HbSS mice receiving phosphate-buffered saline (PBS) or Kyn-CKA (10 mg/kg, iv) 30 min before LPS (0.1 μg/kg, iv). Control, $n = 4$ (89 FOVs); Kyn-CKA, $n = 3$ (60 FOVs). (**L**) Representative FOVs for HbSS mice treated as in (K). Asterisks denote alveolar spaces, arrows indicate blood flow direction, and ellipses show pulmonary vaso-occlusions. Scale bars, 25 μm. $^*P < 0.05$, $^{**}P < 0.01$, $^{***}P < 0.0001$ by *t* test (B, C, G, and I), Mann-Whitney test (F, H, J, and K), or one-way ANOVA and Tukey's test (E).

electrophile discovery involve the use of specific LC-MS/MS and liquid chromatography–high-resolution mass spectrometry (LC-HRMS) detection of proximal metabolites such as nonelectrophilic reaction products, GSH adducts, and excreted urinary conjugates (*30*–*33*). This approach allowed us to identify several specific Kyn-CKA metabolites in vivo: the nonelectrophilic Red-Kyn-CKA in plasma, an intracellular GSH-Kyn-CKA conjugate, and the corresponding cysteine- and *N*-acetyl-cysteine adducts in urine. Unequivocal identification of these metabolites is supported by coelution with isotopically labeled standards for thiol-Kyn-CKA adducts, confirmation of molecular composition, and fragmentation analyses at the <2 parts per million (ppm) level using LC-HRMS. The observation that Red-Kyn-CKA, Cys-Kyn-CKA, and GSH-Kyn-CKA are present in plasma, urine, and liver extracts from untreated mice and healthy humans demonstrates that Kyn-CKA is an endogenous mediator produced in vivo under normal physiological conditions.

Electrophilic molecules such as Kyn-CKA covalently modify hyperreactive and functionally important cysteine thiols in transcription factors, signaling proteins and enzymes to induce changes in protein and cellular function. Nucleophilic targets susceptible to electrophilic addition reactions include the Nrf2 inhibitor protein Keap1 and critical components of the TLR/NF-κB signaling pathway and the NLRP3 inflammasome (*11*, *12*). We show that Kyn-CKA promotes the expression of heme oxygenase 1 (HO1), the glutamate-cysteine ligase regulatory subunit (GCLM), and NAD(P) H:quinone oxidoreductasa 1 (NQO1) in an Nrf2-specific manner, as Kyn-CKA failed to up-regulate these genes in *Nrf2*$^{-/-}$ MEF. Furthermore, Kyn-CKA exhibited potent inhibitory effects on the NF-κB pathway, resulting in decreased expression of LPS-induced proinflammatory and prooxidant genes. Mechanistically, Kyn-CKA interfered with p65 DNA binding as observed with other thiol-reactive electrophiles, thus potentially inhibiting transcriptional activity and favoring p65 reequilibration toward the cytoplasm (*34*, *35*). In line with this observation, Kyn-CKA decreased nuclear p65 levels following LPS challenge without affecting early IκBα degradation kinetics. The complex nature of NF-κB pathway regulation and the promiscuous reactivity of thiol modifying electrophiles suggest that additional mechanisms may also contribute to the anti-inflammatory actions of Kyn-CKA (*36*, *37*). In this regard, Kyn-CKA induced AhR-dependent gene expression in hepatocytes potentially through the formation of quasi-planar metabolites such as Kyn-Yellow. This observation is consistent with a recent report indicating that AhR activation by kynurenine is dependent on the formation of polycyclic derivatives (*22*). Despite the negative regulation exerted by AhR on NF-κB-activation (*38*, *39*), the anti-inflammatory actions of Kyn-CKA in J774a.1 macrophages were AhR independent, and neither Kyn-Yellow nor the canonical AhR ligand TCDD were able to recapitulate the anti-inflammatory effects of Kyn-CKA. Nevertheless, the observation that Kyn-CKA induced AhR-dependent gene expression in BMDM suggests a potential role for Kyn-CKA in AhR-dependent immunomodulatory responses in dendritic and T cells (*2*, *4*, *5*, *40*).

Reactive electrophiles can only act as bona fide signaling mediators if their endogenous concentrations are sufficient to engage their targets in vivo. Cell culture experiments suggest that the concentrations of Kyn-CKA required to elicit biological actions range between 15 and 30 μM. However, Kyn-CKA is a charged amino acid metabolite and thus is unable to move across cellular membranes freely. As a result, cellular responses to exogenous Kyn-CKA are determined not only by its intrinsic reactivity but also by the expression of membrane transporters and competition with other amino acids in the extracellular milieu. To better illustrate the issue of potency versus cell permeability, we designed and synthesized a cell-permeable Kyn-CKA analog by introducing an octanoyl side chain to the aromatic amine via an amide linkage, a common strategy for increasing the cellular permeability of charged compounds (*41*). Treatment of AML-12 cells with *N*-octanoyl-Kyn-CKA resulted in significant induction of Nrf2-dependent gene expression at much lower concentrations (1 to 5 μM) than the impermeable precursor Kyn-CKA. Moreover, we were able to demonstrate that tryptophan addition to AML-12 cells in doses that result in intracellular GSH-Kyn-CKA levels between 100 and 150 nM were sufficient to activate Nrf2-dependent gene expression. Together, these results strongly suggest that intracellular Kyn-CKA yields are likely sufficient to mediate biologically relevant signaling actions in vivo. In this regard, the observation that 100-fold lower doses of either *N*-formylkynurenine or L-Kyn yield similar levels of intracellular GSH-Kyn-CKA to those obtained with tryptophan indicates that kynurenine availability is the rate-limiting factor in Kyn-CKA formation.

Administration of Kyn-CKA in vivo elicited robust signaling responses in the kidney and heart but less so in other tissues such as the liver, lungs, and brain. In the kidney, Kyn-CKA induced Nrf2-regulated gene expression, attenuated proinflammatory genes, and decreased the expression of the renal injury marker *KIM-1* upon LPS challenge. These observations are consistent with the role of this organ in (i) kynurenine reabsorption and metabolism, (ii) Kyn-CKA excretion as urinary Cys-Kyn-CKA conjugates, and (iii) the protective effect of Nrf2 inducers against diverse renal injuries (*42*, *43*). Overall, the differential expression of transporters across cell types and tissues is likely to have a major impact in determining the effects of exogenous Kyn-CKA in vivo. Having demonstrated the endogenous nature and robust signaling actions of Kyn-CKA, it is also shown that Kyn-CKA synthesis is up-regulated under clinically relevant inflammatory conditions and affects complex pathological responses. SCD was selected because of its chronic inflammatory nature, reports of elevated plasma kynurenine levels in patients, and a precedent for reactive electrophiles being able to modulate disease outcome (*19*, *44*, *45*). In line with published results (*44*), plasma kynurenine levels were elevated in both a murine SCD model and patients with SCD, which was in turn associated with increased urinary Cys-Kyn-CKA and plasma Red-Kyn-CKA. Moreover, a strong positive correlation was observed between hemin and kynurenine levels in plasma, indicating that pathologic events in SCD promote kynurenine pathway up-regulation possibly through a combination of direct and indirect effects of hemin on IDO1 and TDO2 expression (*2*, *46*). The heightened inflammatory state of SCD results from up-regulated TLR4 expression, release of proinflammatory hemoglobin-derived products during intravascular hemolysis, and increased gut endotoxin leakage (*47*–*50*). In this context, TLR4 activation by hemin and LPS in endothelial and immune cells and NLRP3 inflammasome engagement in platelets are critical to the onset of vaso-occlusive crises (*21*, *47*, *51*, *52*). Considering the observed anti-inflammatory effects of Kyn-CKA, it was hypothesized that the up-regulation of the kynurenine pathway in SCD constitutes a feedback mechanism to minimize the occurrence of vaso-occlusive events through Kyn-CKA formation. To test this concept, SCD mice were supplemented with Kyn-CKA, and the formation of LPS-induced microvascular obstructions in the pulmonary circulation was quantified in real time by intravital microscopy. Consistent with this hypothesis, increasing systemic Kyn-CKA levels before LPS challenge significantly reduced the size of neutrophil-platelet aggregates and attenuated microvascular occlusions. This effect was likely due to combined inhibitory effects on endothelial adhesion molecule expression and on NF-κB and NLRP3-dependent pathway engagement in myeloid cells and platelets.

Despite the anti-inflammatory effects of Kyn-CKA, significant associations have been found between increased plasma kynurenine levels and poor outcomes in different human diseases (*6*–*9*). However, while these findings have often led investigators to assume that kynurenine synthesis up-regulation is a pathological process, evidence suggests that these responses are a part of a compensatory anti-inflammatory reaction to the specific pathological condition (*10*, *53*). For instance, while genetic IDO1 ablation potentiates antitumor activity and inhibits metastasis (*54*), this same intervention worsens autoimmune disease (*55*). Furthermore, *IDO1* gene

transfer enhances tissue engraftment and survival in an allogenic transplantation model (*56*), and exogenous kynurenine administration is protective against mortality due to severe endotoxemia (*2*). Considering the present results, we propose that the up-regulation of the kynurenine pathway is an adaptive signaling response that suppresses inflammation and protects tissues from injury via Kyn-CKA formation. In summary, this report provides unequivocal evidence that Kyn-CKA is an endogenous mediator that contributes to the immunoregulatory effects of kynurenine and its metabolites, thus affecting disease progression in chronic inflammatory conditions.

MATERIALS AND METHODS

Materials

Antibodies

NLRP3 (catalog no. 15101), IL-1β (catalog no. 12242), inducible nitric oxide synthase (iNOS) (catalog no. 13120), p65 (catalog no. 8242), IκBα (catalog no. 4812), phospho-IκBα (catalog no. 2859), Lamin-B1 (catalog no. 12586), and glyceraldehyde-3-phosphate dehydrogenase (GAPDH) (catalog no. 2118) were purchased from Cell Signaling Technology (Danvers, MA). HO1 (catalog no. ADI-SPA-895) was from Enzo Life Sciences (Farmingdale, NY). NQO1 (catalog no. ab34173) and VCAM-1 (catalog no. ab134047) were from Abcam (Cambridge, UK). GCLM (catalog no. 14241-1-AP) was from Proteintech (Rosemont, IL).

Primers

IL1B (Mm00434228), *IL6* (Mm00446190), *MCP1* (Mm00441242), *HO1* (Mm00516005), *NQO1* (Mm01253561), *GCLM* (Mm01324400), *iNOS* (Mm004405021), *CYP1A1* (Mm00487218), and *CYP1B1* (Mm00487229) were from Thermo Fisher Scientific (Waltham, MA). *KIM-1* (catalog no. 12001950) was from Bio-Rad (Hercules, CA), and *Actin* (catalog no. 4351315) was from Applied Biosystems (Waltham, MA).

Reagents

Probenecid was from Enzo Life Sciences, L-tryptophan-d_3 and $^{13}C_3$-cysteine were from Toronto Research Chemicals (Toronto, Canada); interferon-γ was from BD Pharmingen (Franklin Lakes, NJ); recombinant NF-κB–p65 protein was from Active Motif (Carlsbad, CA); $^{13}C_2$,^{15}N-GSH was from Sigma-Aldrich (St. Louis, MO); and Kyn-CKA [4-(2-aminophenyl)-4-oxobut-2-enoic acid] was custom-synthesized by Toronto Research Chemicals ($\varepsilon_{390\ nm}$ = 3871 M^{-1} cm^{-1}). ^{15}N,$^{13}C_2$-GSH and $^{13}C_3$-cysteine conjugates of Kyn-CKA were generated by reacting 100 equivalents of thiol with Kyn-CKA in 5 mM ammonium bicarbonate (pH 8.0) for 1 hour at 37°C, followed by solid-phase extraction using HyperSep C18 cartridges (Thermo Fisher Scientific). L-Kyn and *N*-formylkynurenine stocks were treated with 35 mg of 3-mercaptopropyl–functionalized silica from SiliCycle (Quebec City, Canada) for 15 min at room temperature to remove potential Kyn-CKA traces, followed by 0.22-μm filtration. Organic solvents were LC-MS grade (Thermo Fisher Scientific), and all other chemicals were of analytical grade and obtained from Sigma-Aldrich unless specified.

Chemical syntheses

General methods

All glassware was oven-dried before use, and reactions were performed under an atmosphere of dry N_2. Acro-seal dry solvents stored over molecular sieves were purchased and used as received. Flash chromatography was performed by a RediSep Combiflash on prepacked cartridges of 40- to 63-μm silica gel. Purity of products was also assessed by high-performance liquid chromatography (HPLC)–UV using C18 reversed-phase column (2 mm by 100 mm, 5 μm; Phenomenex, Torrance, CA) at 220 nm.

Red-Kyn-CKA [(E)-4-(2-aminophenyl)-4-oxobutanoic acid]

A culture tube charged with 23 mg of (*E*)-4-(2-nitrophenyl)-4-oxobut-2-enoic acid (0.1 mmol; synthesis described below) and Pd/C [10% (w/w), 4 mg] was washed in with 2 ml of absolute ethanol. The suspension was stirred and sparged briefly with N_2, and then a H_2 balloon with a three-way valve was attached via a needle through a septum. The solution was evacuated with house vacuum, refilled with H_2 twice, and then stirred 1 hour under H_2 balloon pressure at room temperature. The balloon was refilled when empty (one to two times). After 1 hour, the balloon was removed, and the suspension was filtered through Celite. The solvent was evaporated with a stream of N_2, then the residue was purified by chromatography (silica gel, dichloromethane + 1% HOAc, 0 to 10% MeOH), and the solvent was removed by rotary evaporation to afford 7 mg of final product (36%) matching reported spectra (*57*). ^{1}H nuclear magnetic resonance (NMR) (600 MHz, $CDCl_3$) δ: 7.75 ppm (d, *J* = 8.0 Hz, 1*H*), 7.27 ppm (d, *J* = 8.4 Hz, 1*H*), 6.66 ppm (d, *J* = 7.1 Hz, 1*H*), 6.65 ppm (d, *J* = 7.9 Hz, 1*H*), 3.32 ppm (t, *J* = 6.3 Hz, 2*H*), and 2.76 ppm (t, *J* = 6.4 Hz, 2*H*). ^{13}C NMR (150 MHz, $CDCl_3$) δ: 199.7, 178.2, 150.3, 134.5, 130.8, 117.4, 117.4, 115.9, 33.6, and 28.2 ppm.

(E)-4-(2-nitrophenyl)-4-oxobut-2-enoic acid

(*E*)-4-(2-nitrophenyl)-4-oxobut-2-enoic acid was prepared according to literature procedures and matched to reported spectra (*57*, *58*). Briefly, 2-nitroacetophenone (165 mg, 1.0 mmol) was charged to a 10-ml culture tube along with 92 mg of glyoxalic acid monohydrate (1.0 mmol, 1 eq.) and 2 ml of glacial acetic acid. The tube was covered with a septum with a needle inlet and placed in a preheated sand bath (100° to 110°C), monitored by thin-layer chromatography (TLC), for 24 to 48 hours. After 2 days, HPLC indicated consumption of starting material. The acetic acid was evaporated with a stream of N_2, and then the residue was purified by chromatography (silica gel, dichloromethane + 2% HOAc isocratic). Product fractions were combined, and the solvent was removed by rotary evaporation to provide 151 mg (68%) of pale purple powder. ^{1}H NMR [600 MHz, d_6–dimethyl sulfoxide (DMSO)] δ: 8.24 ppm (d, *J* = 8.2 Hz, 1*H*), 7.93 ppm (t, *J* = 7.5 Hz, 1*H*), 7.83 ppm (t, *J* = 7.8 Hz, 1*H*), 7.71 ppm (d, *J* = 7.5 Hz, 1*H*), 7.21 ppm (d, *J* = 16.0 Hz, 1*H*), and 6.38 ppm (d, *J* = 16.0 Hz, 1*H*). ^{13}C NMR (150 MHz, d_6-DMSO) δ: 192.2, 166.0, 146.2, 138.3, 134.9, 134.4, 134.1, 132.0, 129.0, and 124.7 ppm.

N-octanoyl-Kyn-CKA [(E)-4-(2-octanamidophenyl)-4-oxobut-2-enoic acid]

To a solution of *n*-octanoic acid (160 mg, 1.11 mmol) in dichloromethane was added oxalyl chloride (378 μl, 559 mg, 4.44 mmol) and dimethylformamide (one drop). The mixture was stirred at room temperature for 30 min before being concentrated under vacuum. The resulting oil was redissolved in dichloromethane. To this solution was added (*E*)-4-(2-aminophenyl)-4-oxobut-2-enoic acid (12 mg, 0.063 mmol) and triethylamine (20 μl, 15 mg, 0.14 mmol). The reaction was stirred at room temperature for 30 min before being quenched with 0.1 N of HCl. The mixture was then extracted three times with dichloromethane (15 ml). The combined organic layers were dried, evaporated, and purified by SiO_2 column (from hexanes to 1:1 ethyl acetate/hexanes) to yield the desired acylation product (13 mg, 65%). ^{1}H NMR (500 MHz, $CDCl_3$) δ: 11.48 ppm (s, 1*H*), 8.79 ppm (d, *J* = 8 Hz, 1*H*), 8.05 ppm (d, *J* = 15 Hz, 1*H*),

7.91 ppm (d, J = 8 Hz, 1*H*), 7.63 ppm (t, J = 8 Hz, 1*H*), 7.17 ppm (t, J = 8 Hz, 1*H*), 6.87 ppm (d, J = 15 Hz, 1*H*), 2.48 ppm (t, J = 8 Hz, 2*H*), 1.77 ppm (m, 2*H*), 1.33 ppm (m, 9*H*), and 0.88 ppm (t, J = 7 Hz, 3*H*). ^{13}C NMR (125 MHz $CDCl_3$) δ: 192.4, 173.1, 169.4, 141.8, 139.4, 136.2, 131.7, 131.4, 122.5, 121.6, 121.3, 38.8, 31.7, 29.2, 29.0, 25.5, 22.6, and 14.1 ppm.

Kyn-Yellow (4-oxo-1,2,3,4-tetrahydroquinoline-2-carboxylic acid)

Kyn-Yellow was prepared according to literature procedures and matched reported spectra (*57*). A solution of sodium bicarbonate (0.621 g) and sodium carbonate (0.274 g) was dissolved in 100.0 ml of deionized water to make 0.1 M buffer (pH 9.5). D,L-Kynurenine (49 mg, 0.25 mmol) was charged to a 25-ml round-bottom flask and 10 ml of bicarbonate buffer added, then sealed under a condenser and septum with an N_2 needle inlet, and placed in a preheated sand bath, 100° to 120°C, overnight. The next day, a new fluorescent spot was apparent by TLC. The flask was removed and cooled to room temperature, and the pH value was adjusted to neutral with 0.1 M HCl, then partitioned, and extracted three times with 10 ml of EtOAc. The organic layers were combined, washed twice with 5 ml of brine, and then dried over anhydrous sodium sulfate. The solution was filtered through a plug of Celite/silica gel, and the solvent was removed by rotary evaporation to minimum and then purified by preparatory thin-layer chromatography (EtOAc/toluene/formic acid, 5:4:1). The product band was cut and extracted with elution mixture, and then the solvent was removed by rotary evaporation to provide 21 mg (43%) of intense yellow powder. ^{1}H NMR (600 MHz, d_6-acetone) δ: 7.66 ppm (d, J = 7.9 Hz, 1*H*), 7.31 ppm (t, J = 7.6 Hz, 1*H*), 6.96 ppm (d, J = 8.2 Hz, 1*H*), 6.67 ppm (t, J = 7.4 Hz, 1*H*), 4.40 ppm (t, J = 6.7 Hz, 1*H*), 2.92 ppm (dd, J = 16.3, 5.1 Hz, 1*H*), and 2.84 ppm (dd, J = 16.2, 8.3 Hz, 1*H*). ^{13}C NMR (150 MHz, d_6-acetone) δ: 191.9, 173.1, 152.2, 135.9, 127.4, 119.5, 118.1, 117.2, 55.1, and 40.6 ppm.

Cell culture

The murine hepatocyte AML-12 cell line [American Type Culture Collection (ATCC), CRL-2254] was cultured in Dulbecco's modified Eagle's medium (DMEM)/F12 (1:1) supplemented with 10% fetal bovine serum (FBS), ITS [insulin (10 μg/ml), transferrin (5 μg/ml), and selenite (6.7 ng/ml)] (R&D Systems), dexamethasone (40 ng/ml), penicillin (100 U/ml), and streptomycin (100 μg/ml) at 37°C and 5% CO_2. J774a.1 macrophages (ATCC, TIB-67) were cultured in DMEM containing 10% FBS, penicillin (100 U/ml), and streptomycin (100 μg/ml). Murine BMDMs were isolated from tibia and femur of C57BL/6J mice by flushing the bone marrow with DMEM, high glucose, containing 10% FBS. Cells were differentiated over 7 days in complete medium (DMEM, high glucose, containing 10% FBS and 10% L929 supernatant, 1× nonessential amino acids, 100 μM Hepes, 10 mM glutamine, 1% penicillin/streptomycin, and 50 μM β-mercaptoethanol). L929 cells were cultured in DMEM with 10% FBS + penicillin (100 U/ml) and streptomycin (100 μg/ml). Human pulmonary microvascular endothelial cells (HMVEC-L, Lonza, CC2527) were maintained in VascuLife VEGF-Mv medium (Lifeline, LS-1029). MEFs from *Nrf2*$^{+/+}$ and *Nrf2*$^{-/-}$ mice were a gift from T. Kensler and were maintained as described (*59*).

Real-time polymerase chain reaction

RNA was isolated from cells or pulverized tissues using TRIzol reagent (Invitrogen, USA) (0.4 ml per 1 × 10^6 cells or 1 ml/100 mg of tissue). RNA was quantified by UV absorbance at 260 nm, and cDNA was obtained by reverse transcription using an iScript cDNA kit (Bio-Rad) following the manufacturer's instructions. Reverse transcription polymerase chain reaction (RT-PCR) was performed on StepOnePlus qPCR system using TaqMan Fast Advanced Master Mix (Thermo Fisher Scientific) and the primers listed above. All data were calculated using the relative quantification method ($\Delta\Delta C_t$), and results were expressed as the ratio of the gene of interest to actin expression.

Nrf2-dependent targets

Cells were seeded in a 12-well plate in complete medium (0.5 × 10^6 per well). After reaching confluence, cells were treated with 0 to 60 μM Kyn-CKA ($\varepsilon_{392\,nm}$ = 3871 M^{-1} cm^{-1}), Kyn-Yellow ($\varepsilon_{379\,nm}$ = 4160 M^{-1} cm^{-1}), or 0 to 15 μM *N*-octanoyl-Kyn-CKA ($\varepsilon_{358\,nm}$ = 4893 M^{-1} cm^{-1}) in complete medium without FBS for 8 hours at 37°C and 5% CO_2, followed by RNA isolation and RT-PCR analysis as described.

NF-κB–dependent targets

J774a.1 macrophages or BMDM were seeded in 12-wells plates in complete medium. Confluent cells were preincubated with Kyn-CKA (15 to 60 μM in complete medium without FBS) for 40 min, followed by LPS challenge (*Escherichia coli* O111:B4, 1 μg/ml) for 4 or 8 hours at 37°C and 5% CO_2. Cells were collected in TRIzol reagent and processed for RT-PCR as above.

Protein immunoblotting

Cultured cells were washed twice with cold phosphate-buffered saline (PBS), harvested in 1 ml of PBS, and lysed in 200 μl of radioimmunoprecipitation assay (RIPA) buffer containing EDTA-free protease (Thermo Fisher Scientific) and phosphatase inhibitors (Millipore). Nuclear extracts were prepared using NE-PER (Thermo Fisher Scientific) following the manufacturer's instructions. Flash-frozen and pulverized tissues were resuspended in RIPA buffer (50 mg in 500 μl) containing protease and phosphatase inhibitors as before. Protein concentrations were determined using a BCA Protein Assay Kit (Thermo Fisher Scientific), and equal amounts of proteins were subjected to SDS–polyacrylamide gel electrophoresis using 4 to 12% SDS–polyacrylamide gels. Proteins were transferred to nitrocellulose membranes, blocked with casein in tris-buffered saline for 1 hour at room temperature, and incubated with primary antibodies overnight at 4°C, followed by incubation with horseradish peroxidase–linked secondary antibodies for 1 hour at room temperature. Blots were developed using Clarity Western ECL Substrate in a ChemiDoc XRS$^+$ imaging system (Bio-Rad). Band intensities were quantified using ImageLab 5.0 (Bio-Rad) and normalized to the housekeeping protein GAPDH unless otherwise specified.

Nrf2-dependent protein expression

Cells were seeded in six-well plates (1 × 10^6 cells per well) in complete medium until confluence, followed by incubation with Kyn-CKA (0 to 60 μM) in complete medium without FBS for 16 hours.

NF-κB signaling and NLRP3 engagement

J774a.1 or BMDM (1 × 10^6 cells per well) were pretreated with Kyn-CKA (15 to 60 μM) for 40 min, followed by LPS addition (1 μg/ml for 8 hours). For NLRP3 inflammasome studies, ATP (2 mM) was added in the last 30 min of the incubation.

Human pulmonary microvascular cells

Cells were seeded in a 12-well plate, allowed to grow to confluence, and treated with LPS (100 ng/ml) in the presence of 0 to 60 μM Kyn-CKA for 16 hours.

p65 DNA binding assay

Purified p65 protein (1.5 μM; Active Motif, catalog no. 81086) was filtered through a 10-kDa microcon unit (Millipore), and the buffer

was exchanged with 25 mM Hepes buffer (pH 7.5) to remove tris(2-carboxyethyl)phosphine (TCEP) reductant. The resulting protein was immediately incubated with Kyn-CKA in 25 mM Hepes (pH 7.5) at 37°C, and DNA binding capacity was assessed with the TransAM NF-κB p65 system following the manufacturer's instructions (Active Motif, catalog no. 40096). The final concentration of TCEP in the reaction mixture with Kyn-CKA was estimated at ~1 μM.

Plasma hemin determinations

Hemoglobin-derived species were measured in untreated plasma by nonlinear deconvolution analysis of visible spectra between 520 and 700 nm using Microsoft Excel (*60*). Deconvolution spreadsheets were obtained from R. P. Patel from the University of Alabama at Birmingham.

Extraction of kynurenine and Kyn-CKA metabolites

Cell-based assays

Pellets from L-Kyn, *N*-formylkynurenine (10 and 50 μM; 8 hours at 37°C in HBSS), or tryptophan-treated (0.5 and 5 mM; 8 hours at 37°C in HBSS) cells were washed and lysed in 0.5 ml of MeOH in presence of 100 nM tryptophan-d_3 (Trp-d_3). Lysates were then centrifuged, and supernatants were dried under nitrogen, followed by resuspension in 100 μl of 10% methanol. Medium samples were diluted 1:100 in 10% MeOH in the presence of 500 nM Trp-d_3. When needed, cells were preincubated with probenecid (1 mM) for 1 hour to block MRP function.

In vivo assays

Urine (50 to 200 μl) and plasma (100 μl) samples were deproteinized by addition of 1 ml of cold acetonitrile in the presence of Trp-d_3 internal standard. Samples were incubated for 10 min at −80°C, followed by centrifugation, solvent evaporation, and reconstitution in 10% MeOH. For tissues, frozen pulverized samples were resuspended in 250 μl of water (100 mg/ml) and extracted in 1.5 ml of cold acetonitrile, followed by two cycles of freezing and thawing. Supernatants were dried under nitrogen and reconstituted in 100 μl of water. Trp-d_3 was used as an internal standard at a final concentration of 500 nM.

LC-MS/MS analyses

High-resolution mass spectrometry

Samples were resolved using a reversed-phase HPLC column (2 mm by 100 mm, 5-μm Luna Phenyl-Hexyl, 100-Å column; Phenomenex) and a flow rate of 0.45 ml/min using the following solvent system: A = water/0.1% ammonium acetate/0.2 mM ammonium fluoride (NH_4F) and B = acetonitrile/0.01% formic acid. Samples were loaded at 3.5% B and eluted with a linear increase to 100% organic solvent over 4.9 min. The column was washed with 100% B for 2.3 min and reequilibrated at 3.5% for an additional 2 min. Samples were analyzed using a Q-Exactive hybrid quadrupole-Orbitrap mass spectrometer equipped with an HESI II electrospray source (Thermo Fisher Scientific). Full mass scan analysis ranged from 100 to 600 mass-to-charge ratio at 35,000 resolution. The mass spectrometer analysis was operated in negative mode, with the following parameters: source voltage of 3700 V, spray current of 4 μA, auxiliary gas flow of 15, sheath gas flow rate of 25, sweep gas flow rate of 8, S-lens radio frequency level of 80, and capillary temperature of 320°C. Peak areas were integrated at the MS1 level and normalized to Trp-d_3 internal standard. MS/MS data were used to confirm metabolite identification.

Triple quadrupole mass spectrometry

Metabolite separation was performed using a reversed-phase HPLC column [2 mm by 100 mm, 5-μm C18 Luna (2) column; Phenomenex] at a flow rate of 0.7 ml/min using the following solvent system: A = water/0.2 mM NH_4F and B = acetonitrile/0.01% formic acid. Samples were loaded at 2% B and eluted with a linear gradient from 2 to 100% of B over 4 min. The column was then washed with 100% solvent B for 3 min and reequilibrated at 2% for an additional 5 min. Multiple reaction monitoring mass spectrometry analysis was performed using a Qtrap 6500+ (Sciex) in the negative ion mode with the following parameters: curtain gas of 50, ion spray voltage of −4500 V, temperature of 650°C, ion source gas(1) of 60, ion source gas(2) of 55, and collision gas of −2. The following transitions were used for detection of metabolites and internal standards: kynurenine (207.08/190.0), *N*-formylkynurenine (235.1/190.0), Kyn-CKA (190.0/128.0, 190.0/144.0, and 190.0/146.0), GSH-Kyn-CKA (497.0/306.0), Red-Kyn-CKA (192.1/148.1 and 192.1/92.0), Cys-Kyn-CKA (311.1/120.0 and 311.1/190.0), NAC-Kyn-CKA (369.0/192.0), $^{13}C_3$-Cys-Kyn-CKA (314.1/123.0 and 314.1/190.0) $^{15}N^{13}C_2$-GSH-Kyn-CKA (500.1/309.1), tryptophan (203.1/116.0), and Trp-d_3 (206.1/116.0). Calibration curves were generated using the following extinction coefficients: L-Kyn, $\varepsilon_{360\ nm}$ = 4500 M^{-1} cm^{-1} (sodium phosphate buffer, pH 7.0); *N*-formylkynurenine, $\varepsilon_{321\ nm}$ = 3750 M^{-1} cm^{-1} (sodium phosphate buffer, pH 7.0); GSH-Kyn-CKA, $\varepsilon_{360\ nm}$ = 3889 M^{-1} cm^{-1} (ammonium bicarbonate, pH 8); and Cys-Kyn-CKA, $\varepsilon_{358\ nm}$ = 4893 M^{-1} cm^{-1} (ammonium bicarbonate, pH 8).

Plasma cytokines

Plasma cytokine levels in Kyn-CKA and LPS treated mice were analyzed using an MILLIPLEX MAP Mouse High Sensitivity T Cell Premixed Panel (Millipore) by the Luminex Core Laboratory at the University of Pittsburgh Medical Center (UPMC) Hillman Cancer Center.

Animal studies

All animal experiments were performed with the approval of the Institutional Animal Care and Use Committee of the University of Pittsburgh (19054960 and 19116001).

Kynurenine and Kyn-CKA treatments

Male C57BL/6J mice (RRID:IMSR_JAX:000664), aged 9 to 15 weeks, were injected intraperitoneally with L-Kyn in saline (50 mg/kg) or Kyn-CKA in PBS (20 to 50 mg/kg) for one or two consecutive days. Some mice were challenged with LPS (10 mg/kg, ip) 30 min following Kyn-CKA or vehicle. Urine samples were collected in metabolic cages, volumes were recorded, and creatinine levels were measured using a commercial colorimetric kit (Cayman Chemicals). Plasma and tissues were harvested at the time of sacrifice and flash-frozen in liquid nitrogen. All samples were stored at −80°C.

Intravital lung microscopy

Male and female humanized "Townes" SCD mice (HbSS, homozygous for $Hba^{tm1(HBA)Tow}$ and $Hbb^{tm2(HBG1,HBB*)Tow}$, 8 to 12 weeks; RRID: IMSR_JAX:013071) (*61*) were injected with PBS or Kyn-CKA (10 mg/kg, iv) and then challenged with LPS (0.1 μg/kg, iv) 30 min later. Imaging was performed 3 hours following Kyn-CKA or vehicle as previously (*21*). Mice were anesthetized with ketamine (100 mg/kg, ip) and xylazine (20 mg/kg) followed by cannula insertion into the right carotid artery and tracheotomy to facilitate mechanical ventilation and anesthesia (95% O_2 + 1 to 2% isoflurane). A small portion of the previously exposed left lung was immobilized against

a coverslip using a vacuum-enabled device. Mice were then injected into the carotid artery catheter with fluorescein isothiocyanate–dextran (~125 μg per mouse), AF546-conjugated Ly6G antibody (12 μg per mouse), and V450-CD49b antibody (7 μg per mouse) to visualize the pulmonary microcirculation and the presence of infiltrating neutrophils and platelets, respectively. Time series of two-dimensional fluorescent images (450/20, 525/50, and 576/26 nm) were collected in a Nikon multiphoton-excitation microscope at ~15 frames/s following excitation at 850 nm using a resonant scanner. Each field of view (FOV) was 256 μm by 1256 μm with an *x-y* plane resolution of 0.5 μm per pixel. Imaging was performed for 30 min with each FOV monitored for 30 s. Vaso-occlusions were assessed in at least 20 FOVs per mouse and quantified as the average number of vaso-occlusions per FOV and the average area of each individual vaso-occlusion.

Human subjects

Plasma and urine samples from male and female donors were aliquoted and stored at −80°C within 1 hour of collection (University of Pittsburgh Institutional Review Board CR19030018). Additional age- and race-matched samples from healthy volunteers were obtained from Innovative Research (Novi, MI). Control plasma samples (n = 12) were 50% female, median age of 35 (range: 21 to 62 years), and 100% African descent. SCD plasma samples (n = 10) were 60% female, median age of 39 (*24*–*62*), 90% African descent, 10% white, 60% HbSS, 20% HbSC, 10% $HbSB^+$, and 10% HbSB0. Control urine samples (n = 8) were 50% female, median age of 40 (range, 27 to 62 years), and 100% African descent. SCD urine samples (n = 7) were 71% female, median age 37 (range: 24 to 62), 100% African descent, 71% HbSS, and 29% HbSC.

Statistical analysis

All statistical analysis was performed using Prism 9.1.2 (GraphPad, San Diego, CA). Data were expressed as means ± SD (shown as error bars) and the distributions tested for normality. Differences across normal data populations were examined by either Student's t test or one-way analysis of variance (ANOVA) followed by Tukey's multiple comparison test unless otherwise specified. Nonparametric tests were used for non-normal data distributions. Differences between groups with $P < 0.05$ were deemed significant. Figures show data derived from technical replicates or individual animals and are representative of at least two consistent experiments. Data outliers were identified using the ROUT method with a maximum false discovery rate (s value) of 1%. No exclusion criteria were preestablished.

SUPPLEMENTARY MATERIALS

Supplementary material for this article is available at https://science.org/doi/10.1126/sciadv.abm9138

REFERENCES AND NOTES

1. I. Cervenka, L. Z. Agudelo, J. L. Ruas, Kynurenines: Tryptophan's metabolites in exercise, inflammation, and mental health. *Science* **357**, eaaf9794 (2017).
2. A. Bessede, M. Gargaro, M. T. Pallotta, D. Matino, G. Servillo, C. Brunacci, S. Bicciato, E. M. C. Mazza, A. Macchiarulo, C. Vacca, R. Iannitti, L. Tissi, C. Volpi, M. L. Belladonna, C. Orabona, R. Bianchi, T. V. Lanz, M. Platten, M. A. Della Fazia, D. Piobbico, T. Zelante, H. Funakoshi, T. Nakamura, D. Gilot, M. S. Denison, G. J. Guillemin, J. B. DuHadaway, G. C. Prendergast, R. Metz, M. Geffard, L. Boon, M. Pirro, A. Iorio, B. Veyret, L. Romani, U. Grohmann, F. Fallarino, P. Puccetti, Aryl hydrocarbon receptor control of a disease tolerance defence pathway. *Nature* **511**, 184–190 (2014).
3. F. Fallarino, M. T. Pallotta, D. Matino, M. Gargaro, C. Orabona, C. Vacca, G. Mondanelli, M. Allegrucci, L. Boon, R. Romani, V. N. Talesa, P. Puccetti, U. Grohmann, LPS-conditioned dendritic cells confer endotoxin tolerance contingent on tryptophan catabolism. *Immunobiology* **220**, 315–321 (2015).
4. N. T. Nguyen, A. Kimura, T. Nakahama, I. Chinen, K. Masuda, K. Nohara, Y. Fujii-Kuriyama, T. Kishimoto, Aryl hydrocarbon receptor negatively regulates dendritic cell immunogenicity via a kynurenine-dependent mechanism. *Proc. Natl. Acad. Sci. U.S.A.* **107**, 19961–19966 (2010).
5. M. Hill, S. Tanguy-Royer, P. Royer, C. Chauveau, K. Asghar, L. Tesson, F. Lavainne, S. Rémy, R. Brion, F. X. Hubert, M. Heslan, M. Rimbert, L. Berthelot, J. . R. Moffett, R. Josien, M. Grégoire, I. Anegon, IDO expands human $CD4^+CD25$high regulatory T cells by promoting maturation of LPS-treated dendritic cells. *Eur. J. Immunol.* **37**, 3054–3062 (2007).
6. H. Li, K. Bullock, C. Gurjao, D. Braun, S. A. Shukla, D. Bossé, A. K. A. Lalani, S. Gopal, C. Jin, C. Horak, M. Wind-Rotolo, S. Signoretti, D. F. McDermott, G. J. Freeman, E. M. van Allen, S. L. Schreiber, F. Stephen Hodi, W. R. Sellers, L. A. Garraway, C. B. Clish, T. K. Choueiri, M. Giannakis, Metabolomic adaptations and correlates of survival to immune checkpoint blockade. *Nat. Commun.* **10**, 4346 (2019).
7. H. Zuo, P. M. Ueland, A. Ulvik, S. J. P. M. Eussen, S. E. Vollset, O. Nygård, Ø. Midttun, D. Theofylaktopoulou, K. Meyer, G. S. Tell, Plasma biomarkers of inflammation, the kynurenine pathway, and risks of all-cause, cancer, and cardiovascular disease mortality: The hordaland health study. *Am. J. Epidemiol.* **183**, 249–258 (2016).
8. J. Kaden, D. Abendroth, A. Volp, M. Marzinzig, Dynamics and diagnostic relevance of kynurenine serum level after kidney transplantation. *Ann. Transplant.* **20**, 327–337 (2015).
9. J. C. Schefold, J. P. Zeden, C. Fotopoulou, S. von Haehling, R. Pschowski, D. Hasper, H. D. Volk, C. Schuett, P. Reinke, Increased indoleamine 2,3-dioxygenase (IDO) activity and elevated serum levels of tryptophan catabolites in patients with chronic kidney disease: A possible link between chronic inflammation and uraemic symptoms. *Nephrol. Dial. Transplant.* **24**, 1901–1908 (2009).
10. M. Platten, E. A. A. Nollen, U. F. Rohrig, F. Fallarino, C. A. Opitz, Tryptophan metabolism as a common therapeutic target in cancer, neurodegeneration and beyond. *Nat. Rev. Drug Discov.* **18**, 379–401 (2019).
11. S. Parvez, M. J. C. Long, J. R. Poganik, Y. Aye, Redox signaling by reactive electrophiles and oxidants. *Chem. Rev.* **118**, 8798–8888 (2018).
12. K. V. Swanson, M. Deng, J. P. Ting, The NLRP3 inflammasome: Molecular activation and regulation to therapeutics. *Nat. Rev. Immunol.* **19**, 477–489 (2019).
13. B. D. Hood, B. Garner, R. J. Truscott, Human lens coloration and aging. Evidence for crystallin modification by the major ultraviolet filter, 3-hydroxy-kynurenine O-beta-D-glucoside. *J. Biol. Chem.* **274**, 32547–32550 (1999).
14. B. Garner, D. C. Shaw, R. A. Lindner, J. A. Carver, R. J. Truscott, Non-oxidative modification of lens crystallins by kynurenine: A novel post-translational protein modification with possible relevance to ageing and cataract. *Biochim. Biophys. Acta* **1476**, 265–278 (2000).
15. L. M. Taylor, J. Andrew Aquilina, J. F. Jamie, R. J. Truscott, UV filter instability: Consequences for the human lens. *Exp. Eye Res.* **75**, 165–175 (2002).
16. S. Vazquez, J. A. Aquilina, J. F. Jamie, M. M. Sheil, R. J. Truscott, Novel protein modification by kynurenine in human lenses. *J. Biol. Chem.* **277**, 4867–4873 (2002).
17. L. V. Kopylova, O. A. Snytnikova, E. I. Chernyak, S. V. Morozov, Y. P. Tsentalovich, UV filter decomposition. A study of reactions of 4-(2-aminophenyl)-4-oxocrotonic acid with amino acids and antioxidants present in the human lens. *Exp. Eye Res.* **85**, 242–249 (2007).
18. D. Zhang, C. Xu, D. Manwani, P. S. Frenette, Neutrophils, platelets, and inflammatory pathways at the nexus of sickle cell disease pathophysiology. *Blood* **127**, 801–809 (2016).
19. G. J. Kato, F. B. Piel, C. D. Reid, M. H. Gaston, K. Ohene-Frempong, L. Krishnamurti, W. R. Smith, J. A. Panepinto, D. J. Weatherall, F. F. Costa, E. P. Vichinsky, Sickle cell disease. *Nat. Rev. Dis. Primers.* **4**, 18010 (2018).
20. M. F. Bennewitz, M. A. Jimenez, R. Vats, E. Tutuncuoglu, J. Jonassaint, G. J. Kato, M. T. Gladwin, P. Sundd, Lung vaso-occlusion in sickle cell disease mediated by arteriolar neutrophil-platelet microemboli. *JCI Insight* **2**, e89761 (2017).
21. R. Vats, T. Brzoska, M. F. Bennewitz, M. A. Jimenez, T. Pradhan-Sundd, E. Tutuncuoglu, J. Jonassaint, E. Gutierrez, S. C. Watkins, S. Shiva, M. J. Scott, A. E. Morelli, M. D. Neal, G. J. Kato, M. T. Gladwin, P. Sundd, Platelet extracellular vesicles drive inflammasome–IL-1β–dependent lung injury in sickle cell disease. *Am. J. Respir. Crit. Care Med.* **201**, 33–46 (2020).
22. S. H. Seok, Z. X. Ma, J. B. Feltenberger, H. Chen, H. Chen, C. Scarlett, Z. Lin, K. A. Satyshur, M. Cortopassi, C. R. Jefcoate, Y. Ge, W. Tang, C. A. Bradfield, Y. Xing, Trace derivatives of kynurenine potently activate the aryl hydrocarbon receptor (AHR). *J. Biol. Chem.* **293**, 1994–2005 (2018).
23. P. E. Hanna, M. W. Anders, The mercapturic acid pathway. *Crit. Rev. Toxicol.* **49**, 819–929 (2019).
24. Y. A. Taher, B. J. A. Piavaux, R. Gras, B. C. A. M. van Esch, G. A. Hofman, N. Bloksma, P. A. J. Henricks, A. J. M. van Oosterhout, Indoleamine 2,3-dioxygenase-dependent tryptophan metabolites contribute to tolerance induction during allergen immunotherapy in a mouse model. *J. Allergy Clin. Immunol.* **121**, 983–991.e2 (2008).
25. R. Torosyan, S. Huang, P. V. Bommi, R. Tiwari, S. Y. An, M. Schonfeld, G. Rajendran, M. A. Kavanaugh, B. Gibbs, A. D. Truax, S. Bohney, M. W. Calcutt, E. W. Kerr, R. Leonardi,

P. Gao, N. S. Chandel, P. P. Kapitsinou, Hypoxic preconditioning protects against ischemic kidney injury through the IDO1/kynurenine pathway. *Cell Rep.* **36**, 109547 (2021).
26. J. D. Belcher, C. Chen, J. Nguyen, P. Zhang, F. Abdulla, P. Nguyen, T. Killeen, P. Xu, G. O'Sullivan, K. A. Nath, G. M. Vercellotti, Control of oxidative stress and inflammation in sickle cell disease with the Nrf2 activator dimethyl fumarate. *Antioxid. Redox Signal.* **26**, 748–762 (2017).
27. X. Zhao, G. Sun, J. Zhang, S. M. Ting, N. Gonzales, J. Aronowski, Dimethyl fumarate protects brain from damage produced by intracerebral hemorrhage by mechanism involving Nrf2. *Stroke* **46**, 1923–1928 (2015).
28. M. T. Pallotta, C. Orabona, C. Volpi, C. Vacca, M. L. Belladonna, R. Bianchi, G. Servillo, C. Brunacci, M. Calvitti, S. Bicciato, E. M. C. Mazza, L. Boon, F. Grassi, M. C. Fioretti, F. Fallarino, P. Puccetti, U. Grohmann, Indoleamine 2,3-dioxygenase is a signaling protein in long-term tolerance by dendritic cells. *Nat. Immunol.* **12**, 870–878 (2011).
29. G. Milligan, Orthologue selectivity and ligand bias: Translating the pharmacology of GPR35. *Trends Pharmacol. Sci.* **32**, 317–325 (2011).
30. S. R. Salvatore, D. A. Vitturi, P. R. S. Baker, G. Bonacci, J. R. Koenitzer, S. R. Woodcock, B. A. Freeman, F. J. Schopfer, Characterization and quantification of endogenous fatty acid nitroalkene metabolites in human urine. *J. Lipid Res.* **54**, 1998–2009 (2013).
31. S. R. Salvatore, D. A. Vitturi, M. Fazzari, D. K. Jorkasky, F. J. Schopfer, Evaluation of 10-nitro oleic acid bio-elimination in rats and humans. *Sci. Rep.* **7**, 39900 (2017).
32. J. S. Coukos, R. E. Moellering, Methylglyoxal forms diverse mercaptomethylimidazole crosslinks with thiol and guanidine pairs in endogenous metabolites and proteins. *ACS Chem. Biol.* **16**, 2453–2461 (2021).
33. J. Keller, M. Baradat, I. Jouanin, L. Debrauwer, F. Gueraud, "Twin peaks": Searching for 4-hydroxynonenal urinary metabolites after oral administration in rats. *Redox Biol.* **4**, 136–148 (2015).
34. I. Kastrati, M. I. Siklos, E. L. Calderon-Gierszal, L. el-Shennawy, G. Georgieva, E. N. Thayer, G. R. J. Thatcher, J. Frasor, Dimethyl fumarate inhibits the nuclear factor κB pathway in breast cancer cells by covalent modification of p65 protein. *J. Biol. Chem.* **291**, 3639–3647 (2016).
35. T. Cui, F. J. Schopfer, J. Zhang, K. Chen, T. Ichikawa, R. S. Baker Paul, C. Batthyany, B. K. Chacko, X. Feng, R. P. Patel, A. Agarwal, B. A. Freeman, Y. E. Chen, Nitrated fatty acids: Endogenous anti-inflammatory signaling mediators. *J. Biol. Chem.* **281**, 35686–35698 (2006).
36. J. A. Prescott, J. P. Mitchell, S. J. Cook, Inhibitory feedback control of NF-κB signalling in health and disease. *Biochem. J.* **478**, 2619–2664 (2021).
37. F. J. Schopfer, C. Cipollina, B. A. Freeman, Formation and signaling actions of electrophilic lipids. *Chem. Rev.* **111**, 5997–6021 (2011).
38. A. Kimura, T. Naka, T. Nakahama, I. Chinen, K. Masuda, K. Nohara, Y. Fujii-Kuriyama, T. Kishimoto, Aryl hydrocarbon receptor in combination with Stat1 regulates LPS-induced inflammatory responses. *J. Exp. Med.* **206**, 2027–2035 (2009).
39. Y. Tian, S. Ke, M. S. Denison, A. B. Rabson, M. A. Gallo, Ah receptor and NF-kappaB interactions, a potential mechanism for dioxin toxicity. *J. Biol. Chem.* **274**, 510–515 (1999).
40. J. D. Mezrich, J. H. Fechner, X. Zhang, B. P. Johnson, W. J. Burlingham, C. A. Bradfield, An interaction between kynurenine and the aryl hydrocarbon receptor can generate regulatory T cells. *J. Immunol.* **185**, 3190–3198 (2010).
41. S. Jana, S. Mandlekar, P. Marathe, Prodrug design to improve pharmacokinetic and drug delivery properties: Challenges to the discovery scientists. *Curr. Med. Chem.* **17**, 3874–3908 (2010).
42. S. E. Moller, Pharmacokinetics of tryptophan, renal handling of kynurenine and the effect of nicotinamide on its appearance in plasma and urine following L-tryptophan loading of healthy subjects. *Eur. J. Clin. Pharmacol.* **21**, 137–142 (1981).
43. C. J. Schmidlin, M. B. Dodson, D. D. Zhang, Filtering through the role of NRF2 in kidney disease. *Arch. Pharm. Res.* **43**, 361–369 (2020).
44. S. Sabuncuoğlu, Y. Öztaş, A. Yalcinkaya, S. Ünal, T. Baydar, G. Girgin, The increased neopterin content in turkish pediatric patients with sickle cell anemia. *Ann. Hematol.* **99**, 41–47 (2020).
45. N. Keleku-Lukwete, M. Suzuki, A. Otsuki, K. Tsuchida, S. Katayama, M. Hayashi, E. Naganuma, T. Moriguchi, O. Tanabe, J. D. Engel, M. Imaizumi, M. Yamamoto, Amelioration of inflammation and tissue damage in sickle cell model mice by Nrf2 activation. *Proc. Natl. Acad. Sci. U.S.A.* **112**, 12169–12174 (2015).
46. G. J. Kato, M. H. Steinberg, M. T. Gladwin, Intravascular hemolysis and the pathophysiology of sickle cell disease. *J. Clin. Invest.* **127**, 750–760 (2017).
47. J. D. Belcher, C. Chen, J. Nguyen, L. Milbauer, F. Abdulla, A. I. Alayash, A. Smith, K. A. Nath, R. P. Hebbel, G. M. Vercellotti, Heme triggers TLR4 signaling leading to endothelial cell activation and vaso-occlusion in murine sickle cell disease. *Blood* **123**, 377–390 (2014).
48. G. Chen, D. Zhang, T. A. Fuchs, D. Manwani, D. D. Wagner, P. S. Frenette, Heme-induced neutrophil extracellular traps contribute to the pathogenesis of sickle cell disease. *Blood* **123**, 3818–3827 (2014).
49. E. J. van Beers, Y. Yang, N. Raghavachari, X. Tian, D. T. Allen, J. S. Nichols, L. Mendelsohn, S. Nekhai, V. R. Gordeuk, J. G. Taylor VI, G. J. Kato, Iron, inflammation, and early death in adults with sickle cell disease. *Circ. Res.* **116**, 298–306 (2015).
50. D. Zhang, G. Chen, D. Manwani, A. Mortha, C. Xu, J. J. Faith, R. D. Burk, Y. Kunisaki, J. E. Jang, C. Scheiermann, M. Merad, P. S. Frenette, Neutrophil ageing is regulated by the microbiome. *Nature* **525**, 528–532 (2015).
51. S. Vogel, T. Arora, X. Wang, L. Mendelsohn, J. Nichols, D. Allen, A. S. Shet, C. A. Combs, Z. M. N. Quezado, S. L. Thein, The platelet NLRP3 inflammasome is upregulated in sickle cell disease via HMGB1/TLR4 and Bruton tyrosine kinase. *Blood Adv.* **2**, 2672–2680 (2018).
52. J. D. Beckman, F. Abdullah, C. Chen, R. Kirchner, D. Rivera-Rodriguez, Z. M. Kiser, A. Nguyen, P. Zhang, J. Nguyen, R. P. Hebbel, J. D. Belcher, G. M. Vercellotti, Endothelial TLR4 expression mediates vaso-occlusive crisis in sickle cell disease. *Front. Immunol.* **11**, 613278 (2021).
53. W. D. Hedrich, H. Wang, Friend or foe: Xenobiotic activation of Nrf2 in disease control and cardioprotection. *Pharm. Res.* **38**, 213–241 (2021).
54. X. Zheng, J. Koropatnick, M. Li, X. Zhang, F. Ling, X. Ren, X. Hao, H. Sun, C. Vladau, J. A. Franek, B. Feng, B. L. Urquhart, R. Zhong, D. J. Freeman, B. Garcia, W. P. Min, Reinstalling antitumor immunity by inhibiting tumor-derived immunosuppressive molecule IDO through RNA interference. *J. Immunol.* **177**, 5639–5646 (2006).
55. S. Y. Chen, C. L. Wu, M. D. Lai, C. C. Lin, Y. T. Yo, I. M. Jou, C. H. Lee, C. T. Weng, A. L. Shiau, C. R. Wang, Amelioration of rat collagen-induced arthritis through $CD4^+$ T cells apoptosis and synovial interleukin-17 reduction by indoleamine 2,3-dioxygenase gene therapy. *Hum. Gene Ther.* **22**, 145–154 (2011).
56. K. Iken, K. Liu, H. Liu, P. Bizargity, L. Wang, W. W. Hancock, G. A. Visner, Indoleamine 2,3-dioxygenase and metabolites protect murine lung allografts and impair the calcium mobilization of T cells. *Am. J. Respir. Cell Mol. Biol.* **47**, 405–416 (2012).
57. J. Mizdrak, P. G. Hains, D. Kalinowski, R. J. W. Truscott, M. J. Davies, J. F. Jamie, Novel human lens metabolites from normal and cataractous human lenses. *Tetrahedron* **63**, 4990–4999 (2007).
58. C. L. Xu, X. Bai, J. Xu, J. Ren, Y. Xing, Z. Li, J. Wang, J. Shi, L. Yu, Y. Wang, Substituted 4-oxo-crotonic acid derivatives as a new class of protein kinase B (PknB) inhibitors: Synthesis and SAR study. *RSC Adv.* **7**, 4763–4775 (2017).
59. R. S. Wible, C. Ramanathan, C. H. Sutter, K. M. Olesen, T. W. Kensler, A. C. Liu, T. R. Sutter, NRF2 regulates core and stabilizing circadian clock loops, coupling redox and timekeeping in Mus musculus. *eLife* **7**, e31656 (2018).
60. J. Y. Oh, J. Hamm, X. Xu, K. Genschmer, M. Zhong, J. Lebensburger, M. B. Marques, J. D. Kerby, J. F. Pittet, A. Gaggar, R. P. Patel, Absorbance and redox based approaches for measuring free heme and free hemoglobin in biological matrices. *Redox Biol.* **9**, 167–177 (2016).
61. L. C. Wu, C. W. Sun, T. M. Ryan, K. M. Pawlik, J. Ren, T. M. Townes, Correction of sickle cell disease by homologous recombination in embryonic stem cells. *Blood* **108**, 1183–1188 (2006).

Acknowledgments: We thank N. Wakabayashi for lending expertise for the generation of MEFs from *Nrf2*$^{+/+}$ and *Nrf2*$^{-/-}$ mice. **Funding:** This work was supported by National Institutes of Health grants K01HL133331 (to D.A.V.), R03HL157878 (to D.A.V.), R56AI165479 (to D.A.V.), R01GM125944 (to F.J.S.), R01DK112854 (to F.J.S.), R01HL133864 (to A.C.S.), R01HL128304 (to A.C.S.), R01HL149824 (to A.C.S.), R35HL161177 (to A.C.S.), R01HL058115 (to B.A.F.), R01HL64937 (to B.A.F.), P01HL103455 (to B.A.F.), R01DK124510 (to N.K.H.K.), R01DK124426 (to S.G.), U54HL141011 (to S.O.), R01HL128297 (to P.S.), and R01HL141080 (to P.S.); pilot from National Institutes of Health grant P30DK079307 (to D.A.V.); and American Heart Association grant 19EIA34770095 (to A.C.S.). This publication was also made possible by support from the Vascular Medicine Institute, the Hemophilia Center of Western Pennsylvania (to D.A.V.) and the Institute for Transfusion Medicine and Pittsburgh Liver Research Center (NIH grant P30DK120531). **Author contributions:** Conceptualization: D.A.V., G.J.K., P.S., and F.J.S. Methodology: D.A.V., M.C., M.F.P., S.R.S., S.G.W., T.B., and P.S. Investigation: D.A.V., M.C., M.F.P., S.R.W., T.B., S.G., M.D., N.C., S.Y., N.K.H.K., and F.C. Funding acquisition: D.A.V., S.F.O.-A., B.A.F., F.J.S., A.C.S., and P.S. Project administration: D.A.V. Resources: D.A.V., G.J.K., S.G., S.G.W., S.F.O.-A., B.A.F., F.J.S., and P.S. Supervision: D.A.V., A.C.S., P.S., S.F.O.-A., F.J.S., and B.A.F. Writing (original draft): D.A.V., M.C., and M.F.P. Writing (review and editing): D.A.V., B.A.F., P.S., and F.J.S. **Competing interests:** G.J.K. is an employee of CSL Behring. F.J.S. and B.A.F. acknowledge financial interest in Creegh Pharmaceuticals Inc. P.S. serves on the advisory board of Novartis AG, IHP Therapeutics, and CSL Behring Inc. P.S. has received research funding from Novartis AG, IHP Therapeutics, and CSL Behring Inc. in the form of sponsored research agreements that are not related to the subject of the current study. P.S. is also the recipient of Bayer Hemophilia Basic Science Research Award. The authors declare that they have no other competing interests. **Data and materials availability:** All data needed to evaluate the conclusions in the paper are present in the paper and /or the Supplementary Materials.

Submitted 20 October 2021
Accepted 11 May 2022
Published 29 June 2022
10.1126/sciadv.abm9138